8-24-2011

Implementing a Long-Term Bridge Monitoring Strategy for a Composite Steel Girder Bridge

Shelley Plude
University of Connecticut - Storrs, shelley.plude@gmail.com

Implementing a Long-Term Bridge Monitoring Strategy for a Composite Steel Girder Bridge

Shelley Elizabeth Plude

B.S., University of Connecticut, 2009

A Thesis

Submitted in Partial Fulfillment of the

Requirements for the Degree of

Master of Science

at the

University of Connecticut

2011

APPROVAL PAGE

Master of Science Thesis

Implementing a Long-Term Bridge Monitoring Strategy for a Composite Steel Girder Bridge

Presented by:

Shelley Plude, B.S.

Major Advisor: _____
Dr. Richard Christenson

Associate Advisor: _____
Dr. John T. DeWolf

Associate Advisor: _____
Dr. Jeong-Ho Kim

The University of Connecticut

2011

Acknowledgments

I would like to take this opportunity to thank everyone who has supported me throughout my academic career. First, I would like to thank my parents for making my time here at UConn possible through their never ending support and encouragement. I would also like to thank my friends and fellow graduate students for all of the wonderful experiences over these last few years. Finally, thank you to my advisor, Dr. Richard Christenson, and to my advisory board who have guided me throughout this process. Your assistance and insight have been greatly appreciated.

Table of Contents

CHAPTER 1: Introduction

The University of Connecticut and the Connecticut Department of Transportation have established a long-term bridge health monitoring system to monitor critical vulnerabilities in a group of bridges throughout the state. This research focuses on a single bridge located on I-91 in Cromwell. The bridge is a three-span, simply supported composite steel girder bridge carrying three lanes of highway traffic. It has been a part of the University of Connecticut and Connecticut Department of Transportation monitoring network since 2004 and is fitted with 20 strain gauges located at midspan at the top and bottom of the web of each girder.

In order to monitor the critical vulnerabilities of the bridge, it is important to quantify anticipated changes in measurements resulting from different types and levels of damage. Chapter 2 focuses on the identification of damage measures for the composite steel girder bridge using a finite element model. In this chapter, four damage measures including natural frequency, peak strain, strain distribution, and neutral axis location, will be presented. The changes in these damage measures for five different damage scenarios at various levels of severity will be examined to identify the specific damage measures best suited to identify each particular type of damage.

In order to incorporate these damage measures into the automated bridge monitoring system of this bridge, the anticipated changes in the damage measures observed in Chapter 2 must be compared to the inherent variability of actual bridge measurements to determine the minimum level of damage that can be detected by the system. Chapter 3 focuses on the evaluation of the uncertainty of each damage measure and its sensitivity to damage. This paper describes the process by which a damage

measure's uncertainty is evaluated and its sensitivity to damage compared with the anticipated changes in the damage measure identified by the finite element model. Based on these comparisons, the minimum vulnerability that can be identified by the monitoring system can be determined.

There are four appendices to supplement this thesis. Appendix A is a manual for the finite element model providing detailed descriptions of the procedures and methods used to model this bridge. Appendix B provides a more in-depth explanation of the dynamic truck loading applied to the finite element model. Appendix C contains the complete results of the finite element model discussed in Chapter 2. Appendix D contains additional results from the analysis of the uncertainty of the damage measures.

CHAPTER 2: Identifying Damage Measures for a Composite Steel Girder Bridge Using Finite Element Analysis

Abstract

A long term bridge monitoring program has been established in Connecticut to monitor critical vulnerabilities in bridges. In doing so it is important to quantify anticipated changes in measurements resulting from different types and levels of damage with the intent of comparing these changes to the inherent variability in actual bridge measurements to determine the minimum level of vulnerability that can be identified through bridge monitoring. This is done in a continuous manner over the life of the bridge. This paper focuses on the identification of damage measures for a composite steel girder bridge located on Interstate 91 (I-91) in Connecticut. In this paper, four damage measures including natural frequency, peak strain, strain distribution, and neutral axis location, will be analyzed using a finite element model of the composite steel girder bridge. Five different damage scenarios at various levels of severity are examined using the finite element model. Specific damage measures are then proposed to identify the different anticipated failure modes of the bridge. These damage measures will be incorporated into the automated bridge monitoring system located on the highway bridge.

Introduction

The University of Connecticut and the Connecticut Department of Transportation have been partners in bridge monitoring research for the past twenty years (1-5). Current research efforts focus on the long-term continuous monitoring of six different types of highway bridges located throughout Connecticut (6). The intent of this research is to better understand how to monitor critical vulnerabilities in the State's highway bridges.

Long-term bridge health monitoring can supplement bridge inspections, help to quantify the current structural condition of the bridge, and identify the onset of damage in the structural system (7-8). Continuous monitoring has the potential to identify the presence of damage in a bridge in the early stages before the damage reaches a critical stage or results in the failure of the structure. By examining changes in a bridge's physical characteristics and behavior during operating traffic conditions, using damage measures such as the natural frequency, peak strain, strain distribution, and neutral axis location, it may be possible to determine if damage is present as well as identify the location of the damage. The specific damage measures (DMs), calculated from available bridge response measurements, can be identified for each bridge based on its specific design, use, and critical elements. These DMs can be used to supplement regular visual bridge inspections adding a quantitative measure of the structure's condition. It is important to identify for anticipated damage conditions the most appropriate DMs in a quantitative manner.

The bridge examined in this paper has been part of the University of Connecticut and Connecticut Department of Transportation long-term bridge monitoring network since 2004 (1) and has recently received equipment upgrades including a new data acquisition system and temperature sensors. The bridge is a three-span, simply supported, composite steel girder bridge, with the first two spans monitored using dynamic strain gages. A finite element model of the first simply supported span was developed to quantify the changes in the various damage measures for specific types of damage. In this paper, the bridge and its monitoring system are presented along with the specific DMs identified from previous research (1). Next, a finite element model of the

bridge is presented along with details of the truck loading and five specific damage cases considered in this study as the most likely to occur on this particular bridge. The sensitivity of the DMs are then quantified for the various damage cases in order to identify the most appropriate DM(s) to best identify each type of damage. The specific DMs used to monitor each damage case are then identified for implementation on the in-service composite steel girder bridge long-term monitoring system.

Composite Steel Girder Bridge and Associated Long-Term Monitoring System

The composite steel girder bridge in this study is a three span, simply supported bridge that carries three lanes of I-91 southbound traffic over the Mattabesset River. The bridge is located near the town of Cromwell, Connecticut. This three lane highway bridge has a total length of 216 feet with two inch expansion joints separating each span. The bridge was built in 1965 and reconstructed in 1998.

Only the first span (Span 1) of the bridge is considered in this study. The girders in Span 1 are W36x194 steel sections with 10”x1” partial length cover plates. The diaphragms are C15x33.9 sections and are located at the quarter points. Figure 1 shows an elevation view and cross section view of the bridge.

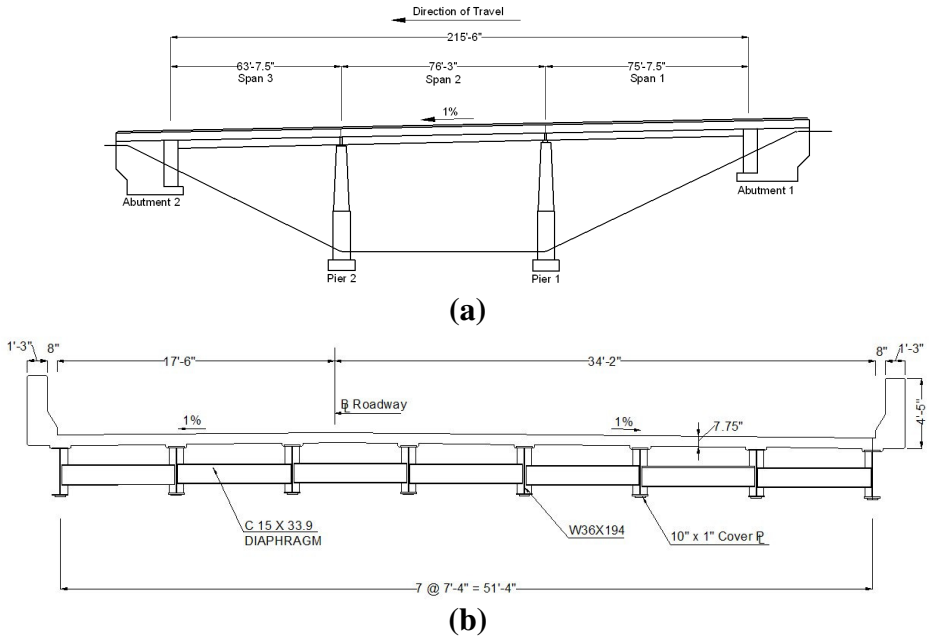

Figure 1. Elevation (a) and Cross Section (b) of the Composite Steel Girder Bridge.

The bridge is currently being monitored by 20 foil-type strain gages attached to the webs of the girders in Spans 1 and 2. A plan view of the bridge including the sensor locations is shown in Figure 2. The sensors are welded on either the top or bottom of the web of the girder. Strain sensors at the bottom of the girder are intended to provide maximum stress/strain measurements. Collocated strain sensors at the top of the web are used, along with the bottom sensor, to determine the location of the neutral axis of the bridge and identify composite action between the girders and bridge deck.

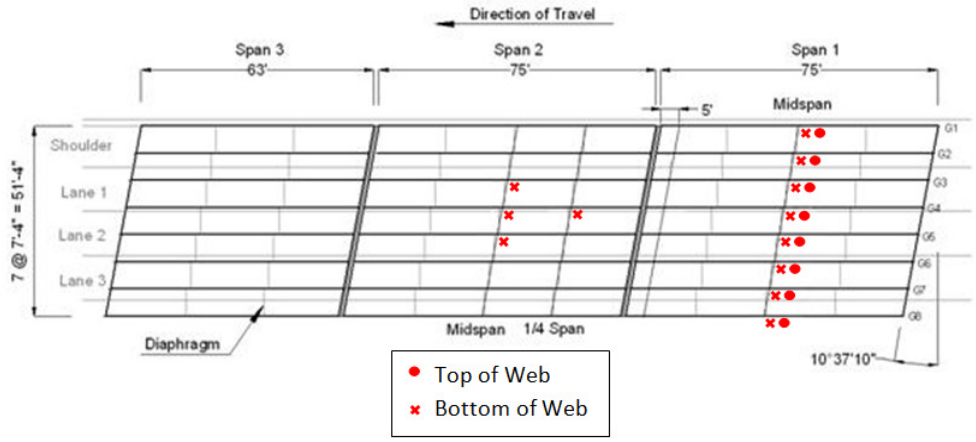

Figure 2. Strain Sensor Locations on the Composite Steel Girder Bridge.

Proposed Damage Measures

Previous research has identified four damage measures (DMs) for this composite steel girder bridge (5). This research will examine the effectiveness of these DMs in detecting specific types of damage that are likely to occur on the bridge. The DMs considered include: fundamental natural frequency; peak strain; strain distribution; and neutral axis location. While environmental and operational variability of bridge structures can affect their dynamic properties and response, it is assumed in this study that any variability is appropriately accounted for, as done by Scianna et al. (9).

The first damage measure is the fundamental natural frequency of the bridge, denoted DM_{ω}. The natural frequency of the bridge is a measure of its dynamic characteristics and is dependent on the physical characteristics of the bridge, namely the mass, stiffness, damping, and the boundary conditions. The presence of damage on the bridge will change any one of these physical characteristics thus producing a change in the fundamental natural frequency.

The next DM is peak strain for each of the girders, denoted $DM_{\varepsilon i}$. The peak strain in each girder is analyzed to determine if there has been any change in behavior in a particular girder's strength as the result of damage or fatigue. This is determined by identifying the maximum strain in the sensors located at the bottom web of each girder as a truck travels over the bridge. Once this maximum strain is identified for a truck crossing, the strain in all eight girders is taken at the same time. Changes in the peak strain values of a girder can be attributed to a change in the capacity of a member or an adjacent member and is indicative of damage in the bridge. The weight of the truck will also have a direct impact on the peak strain. Adoption of bridge weigh-in-motion

(BWIM) techniques can help to identify specific weights of the crossing trucks (5- 6) and account for this variability.

The third damage measure is strain distribution for each of the girders, denoted DM_{dist_i}. To determine the strain distribution factor for each girder, the strain distribution at peak strain is used. The strain in each girder is divided by the sum of the strains in all eight girders to determine what percentage of the load a particular girder is carrying. If a girder becomes cracked or otherwise damaged, the strains in the adjacent girders of this indeterminate system will change due to a redistribution of loads.

The last damage measure examined is the location of the neutral axis for each of the girders, denoted DM_{NAi}. Since the location of the neutral axis is dependent on the strain distribution throughout the cross section, including the slab, changes in the location of the neutral axis can be used to identify damage in either the girders or the adjacent slab. Again, measurements taken at the time of the peak strain are used to determine the location of the neutral axis. The strains in the top and bottom of the web are used to calculate the neutral axis location assuming a linear distribution of strain over the height of the cross-section.

Bridge Finite Element Model

In this paper, a finite element model is used to identify the appropriate DMs to use for specific failure modes. The first span, Span 1, of the composite steel girder bridge is modeled using a three-dimensional finite element model, as shown in Figure 3. The span is assumed to be simply supported. This assumption has been validated by field measurements of adjacent spans (i.e. the strain measurements in Span 2 remain unchanged until the truck on Span 1 enters onto Span 2). The bridge is modeled using

plate elements to best capture the local crack behavior and global structural changes. For the undamaged case the model is comprised of 15,952 nodes and 50,348 plate elements. The number of nodes in the damaged models varies slightly from the undamaged case to physically model the different damage cases using more refined plate elements.

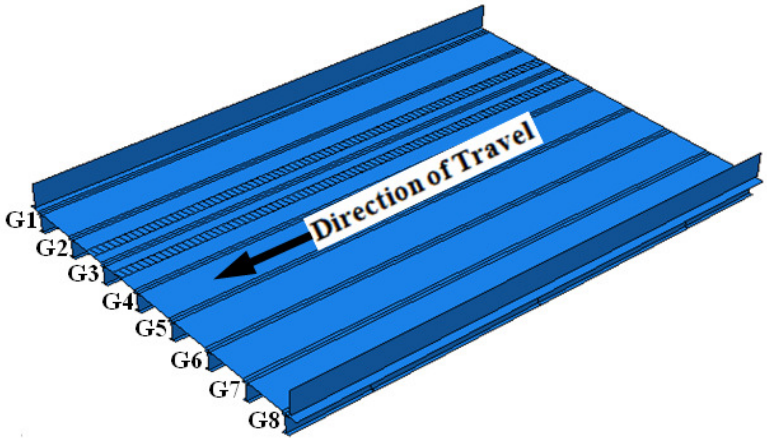

Figure 3. Finite Element Model of Composite Steel Girder Bridge.

The plate elements in the slab and bridge girders were assigned a uniform thickness and material properties, corresponding to the specifications of the composite steel girder bridge. To ensure composite action for the model between the elements in the slab and the elements in the girders, the nodes in the top flanges of the girders were tied to the nodes in the concrete deck. The concrete parapets were modeled by plate elements with a uniform thickness that approximates the weight and dimensions of the actual parapets.

The bridge model is loaded using a five-axle 47ft truck with a 6ft wheelbase and a total weight of 69.76 kips (5). The truck configuration is shown in Figure 4. The truck was positioned so that it straddled Girder 3 to simulate a truck travelling in the right travel lane. The contact area for the tires was based AASHTO specifications and constitutes a moving area of 10 inches by 20 inches (10). Each axle is modeled as a

distributed load over two tire areas. The five axle load pairs of the truck are then incremented over the bridge deck in time corresponding to a vehicle speed of 65 miles per hour (mph). In such a manner the vehicle-bridge dynamic interaction is neglected. The inertial effects of the truck are also neglected in this approximation of the truck loading. Since the mass of the truck is less than 0.9% of the mass of the bridge itself, this is assumed to be a reasonable approximation.

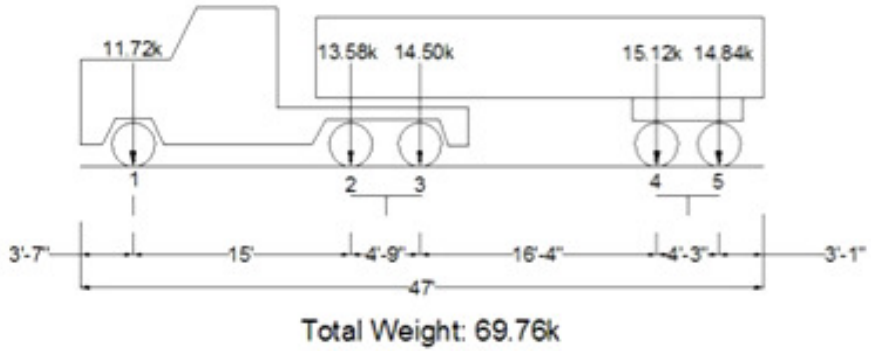

Figure 4. Configuration of Truck Used to Load Bridge.

To verify the finite element model, the response of the undamaged model was compared with measured strain data of a similar truck crossing the bridge (5). Figure 5 shows a comparison of the strain in three of the girders as the truck crosses the bridge. The finite element model yielded peak strains of 55με and 43με in girder 3 (G3) and G4 respectively which corresponds well with the peak strains of 51με and 45με recorded by the monitoring system. The fundamental natural frequencies also match well with 5.14 Hz from the model which fits within the 4.02 and 5.4Hz range calculated from the measured data. The measured data produces a range of values due to a number of factors including environmental variability and noise in the sensor readings which leads to uncertainty in the peak picking method used to calculate the natural frequency. Overall, the model is able to capture the dynamic behavior of the bridge loaded by a 5-axle truck.

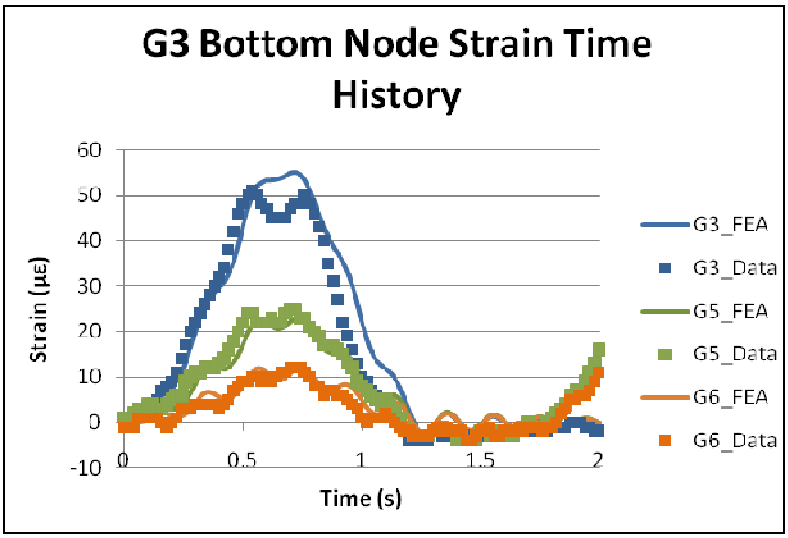

Figure 5. Comparison of Measured and Modeled Bridge Strains.

Bridge Damage

There are many different types of damage a composite steel girder bridge might experience. For this paper, three types of damage are considered: fatigue cracking due to truck traffic; impact of a truck passing under the bridge; and deterioration of the bridge deck. In order to cover these potential damage scenarios, five different cases are considered.

Cases 1 and 2 represent fatigue related damage to the bridge. Cases 3 and 4 capture potential damage as the result of a truck impacting the exterior girder of the bridge. The fifth damage case represents damage to the bridge deck.

Case 1- Cracking in Girder 3 at Midspan: The first damage case was chosen to represent a fatigue crack developing in the area of highest stress on the bridge, the midspan. In this case, the damage is located directly beneath the strain gage which means the damage should be easily detectable even during the early stages of crack development.

Case 2- Cracking in Girder 3 at the End of the Coverplate: The second damage case is representative of a fatigue crack that develops as the result of the discontinuity and stress concentration caused by the end of the partial length coverplate.

Case 3- Cracking in Girder 1 at 1/3rd Span: The third damage case is the first of two designed to simulate damage as the result of a truck impacting the exterior girder. As the result of the impact, damage is introduced to the girder as a crack that will develop slowly over time following the impact event. The crack was placed at 1/3rd span, directly over the slow lane of a roadway travelling under the bridge, to model the location most likely to be susceptible to impact. The location of damage for these first three cases is shown on the finite model in Figure 6.

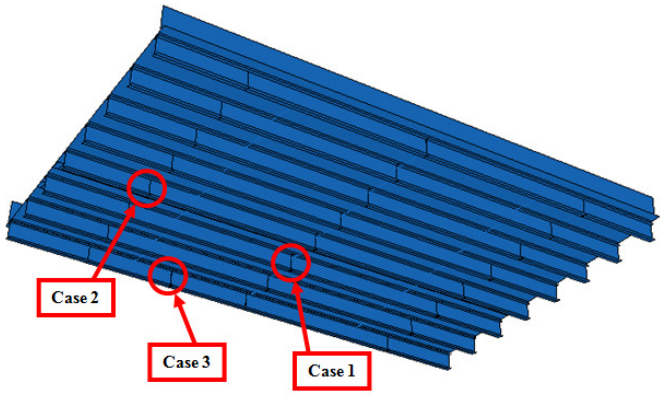

Figure 6. Damage Location for Cases 1, 2, & 3.

For damage cases 1 through 3 where cracking of the girder is involved, a total of four levels of damage were used to model the progression of a 3/8 inch wide crack, as in Farrar et al. (11). Figure 7 shows a drawing of the cross-section of the G3 girder for all four damage levels.

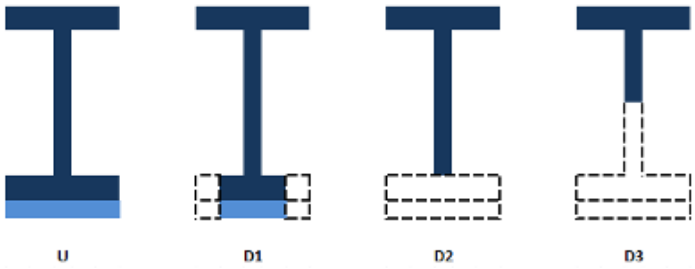

Figure 7. Cross-Section of Damaged Bridge Girder at Damage Location: undamaged (U): 50% reduction in the bottom flange and cover plate (D1): 100% reduction in the bottom flange and cover plate (D2): and 100% reduction in the bottom flange and cover plate and 50% reduction of the web (D3).

Case 4- Loss of Composite Action in Girder: In addition to potential cracking in the exterior girder as the result of a truck impact, it is possible that the girder may become noncomposite as the result of the large horizontal force applied. Three levels of noncomposite action are modeled: one quarter of the girder centered on the impact site at 1/3rd span becomes noncomposite (D1); the half of the girder closest to the impact site becomes noncomposite (D2); and the entire Girder 1 becomes noncomposite (D3).

Case 5- Deck Deterioration: Deck deterioration is a very complex issue that has been the focus of many studies (12-13). Deck deterioration is not usually a localized problem and often affects large portions of a bridge deck. This study will look to model the initiation of deck deterioration as a small patch, 30 inches by 6 feet, located directly under the right travel lane at the quarter span of the bridge. The progressive loss of deck strength is simplified here by reducing the elastic modulus by 25% (D1), 50% (D2) and 75% (D3) of its full strength (626,400 ksf).

Results of Finite Element Analysis

The strains at the top and bottom of the web of each girder at the location of the sensors on the bridge were obtained from the finite element models and used to calculate the four damage measurements. The results of the changes in the DMs for the damage cases using the finite element models are discussed in this section.

The first damage measure examined here is the fundamental natural frequency. Based on the results shown in the figure below, the fundamental natural frequency does not change considerably as the level of damage is increased. For Cases 1-3 and 5, damage is not easily detectable using DM_ω. Even for the most severe level of damage, ΔDM_ω does not exceed 0.1267Hz.

Damage Case 4 (noncomposite behavior of G1) exhibits more significant changes in fundamental natural frequency. For the lowest level of damage, where a quarter of the girder centered around $1/3^{rd}$ span becomes noncomposite, ΔDM_ω is small equaling only 0.1587Hz. When half of the girder becomes detached from the deck, ΔDM_ω jumps to 0.8565Hz and then to 1.8816Hz once the entire girder becomes noncomposite. This sudden jump is due to a local vibration mode of the deck. Once it becomes noncomposite, the girder and deck are allowed to vibrate independently thus producing a more significant change in DM_ω.

Case 5, deck deterioration, produced the smallest change in DM_ω with the largest change in natural frequency occurring for the most severe level of damage resulting in a change of 0.016Hz.

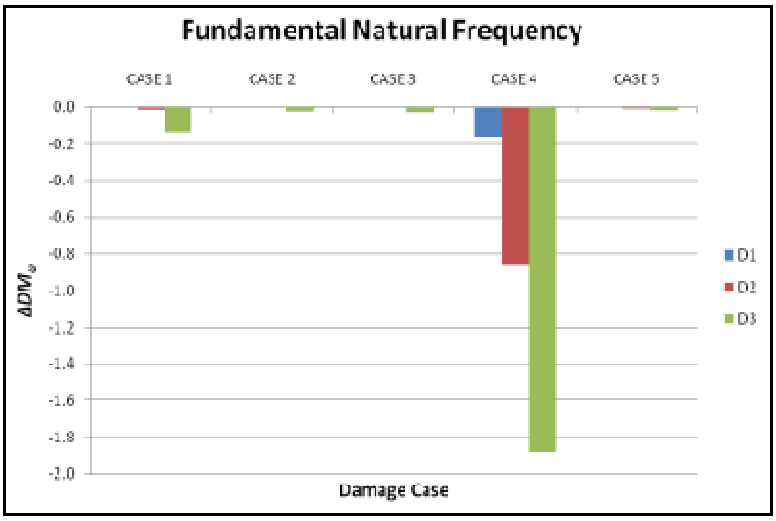

Figure 8. ΔDM_{ω} for All Four Damage Cases

The next DM is peak strain. The maximum strain for the undamaged case is observed to be 55.14με in girder 3 at 0.717 seconds, when the third (14.50 kips) and fourth axles (15.12k) are approximately centered over the sensor location. Figure 9 shows the girders with the most significant changes in DM_{ε} for all five damage cases.

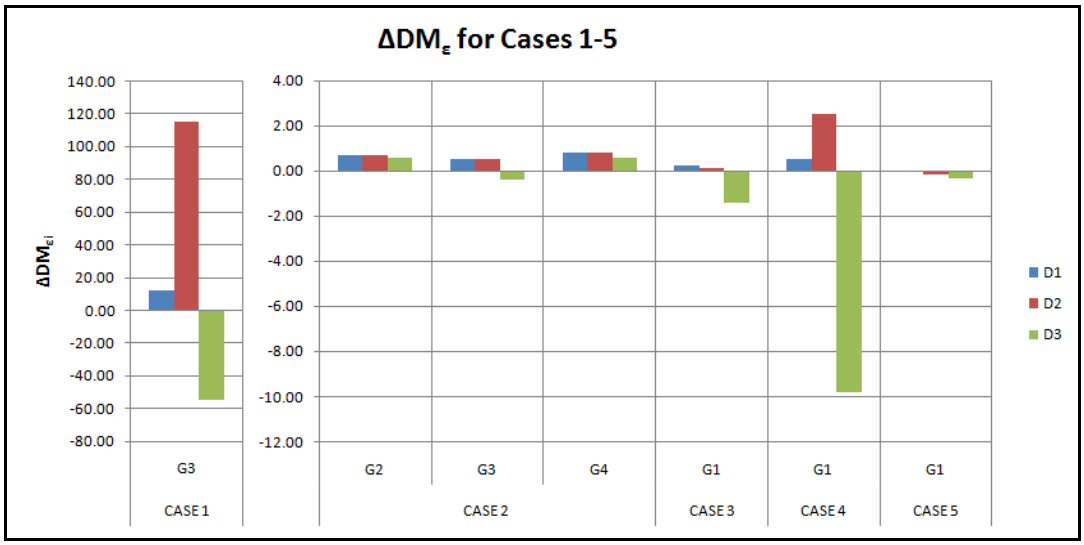

Figure 9. ΔDM_{ε} for Cases 1-5

As evident in Figure 9, a sharp increase in strain is observed in G3 for D1 and D2. With a 50% reduction in the bottom flange the strain increases by 12.01με. As the result of the loss of capacity in the bottom flange as well as the cover plate, the web directly

above the flange crack must pick up more of the load. In damage case D3, the crack has progressed into the web beyond the sensor location therefore resulting a $\Delta DM_{\varepsilon 3}$ equal to the undamaged maximum strain.

Damage Cases 2 and 3 in which the cracks are modeled at some distance from the sensor location allow for further examination of the general case when damage occurs away from a strain sensor. In contrast with the change in $DM_{\varepsilon 3}$ seen for Damage Case 1, the strains at the sensor do not vary significantly between the three damage levels.

For Damage Case 2, where the damage occurs 25.5ft away from the sensor at the end of the coverplate, the most significant changes occur across three girders: G2, G3, and G4. The largest changes are observed in G2 and G4 which have nearly symmetrical changes in strain (0.7 to 0.8με for D1/D2 and 0.6 με for D3) as they pick up more of the load usually carried by G3.

In Damage Case 3, where the damage occurs at 1/3rd span on G1 (12.5ft from the sensor location), the damage is a little more noticeable but only once the crack has progressed through 50% of the web. There is a slight increase in strain in G1 (0.24με) for D1, but it isn't until D3 that the strain suddenly drops by 1.4με.

In Damage Case 4 (noncomposite action of G1), there is a more discernable change in strain. As G1 becomes progressively noncomposite, the strain at midspan in G1 changes by 0.51 (D1), 2.49 (D2), and -9.81με (D3). For D1 and D2, a portion of the girder is still attached to the deck. Therefore, when the truck passes over G3, the load can still be transferred into G1. However, when the exterior girder has become completely detached, the deck is free to move independently of the girder which means

the load cannot be transferred as effectively into the girder leading to lower stresses in G1.

The last remaining damage case (deck deterioration) exhibits little change in peak strain. As shown in Figure 9, the change in the affected girders is negligible. The maximum change observed is 0.34με in G1 and only at the most severe damage level.

The third damage measure is strain distribution. The distribution factors are calculated using the peak strain values by dividing the strain of each girder by the sum of the strains of all eight girders. Since the truck is being driven across the right travel lane directly over G3, this girder takes the majority of the load, with the remainder distributed to the adjacent girders. When the strain sensor is located directly above the damage, the strain distribution, like the peak strain, changes dramatically. Since such large changes in the damage measures for Case 1 would be easily detectible, the next set of figures focuses on Cases 2 through 5.

For Cases 2 and 3 that involve cracking in the girder, the strain distribution, like the peak strain shown in the previous section, changes very little. In both cases, change in percentage of the truck load carried by the damaged girder less than 1.0% for D3. As was the case with peak strain, Case 3 shows a larger change in D3 when compared with Case 2. This is due to the fact that the damage location in Case 3 is closer to the location of the strain sensor (12.5ft) as opposed to 25.5ft for Case 2.

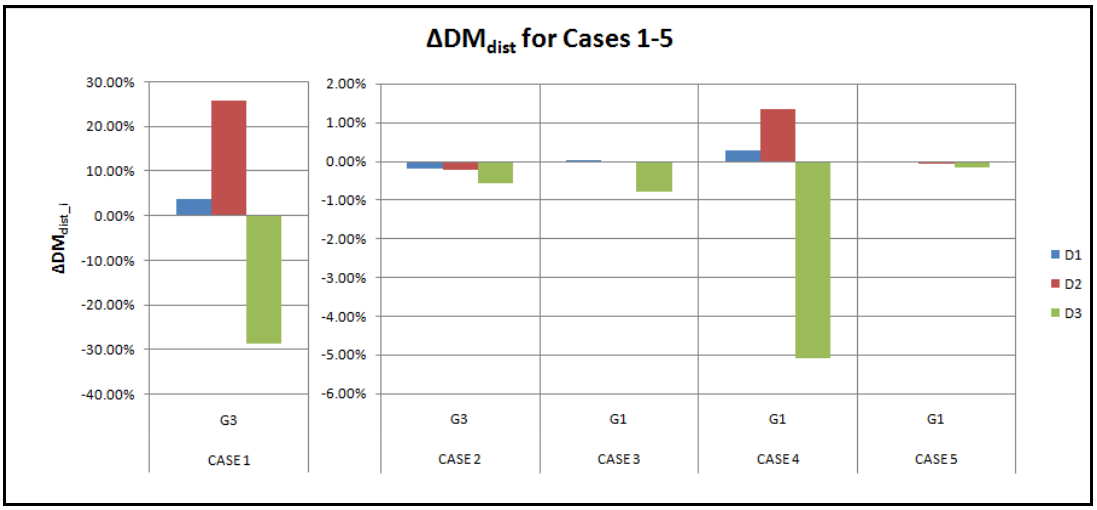

Figure 10. ΔDM_{dist} for Cases 1-5

For Case 4, where G1 becomes noncomposite, the change in strain distribution is more noticeable showing a slight increase in the load carried before dropping 5%.

As was the case with peak strain, strain distribution shows very minimal change for the fifth damage case. The largest changes in distribution are observed in G1 and amount to less than 0.2% decrease in the girder's load distribution.

The fourth damage measure examined is neutral axis location. The neutral axis of each girder was calculated using the strain obtained from the top and bottom web sensors and is measured from the top of the slab. When a truck passes over the bridge in the right lane (centered over G3), the eighth girder is entirely in tension due to the live load and therefore the neutral axis would fall in the slab. While it should be noted that the dead load stresses from the bridge self weight will result in an overall neutral axis in the girder, for instances where the entire cross section, girder and slab, is in tension, the neutral axis could not be calculated and was assumed to be zero.

Figure 11 shows ΔDM_{NA} for Cases 2 through 5. For Cases 2 and 5, DM_{NA} exhibits very minor changes in the neutral axis location. For Case 2, DM_{NA2} shows a very small change of 0.18 inches while DM_{NA1} changes by 0.68 inches for Case 5. Case 3

exhibits a larger change in neutral axis but not until damage level D3 with a 1.5 inch increase in DM_{NA3}.

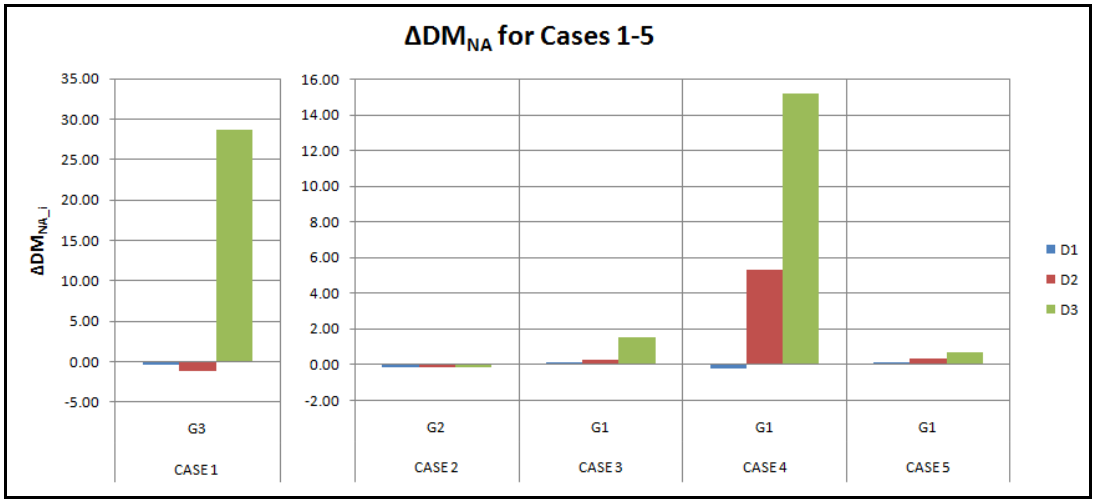

Figure 11. ΔDM_{NA} for Cases 1-5

For Case 4 where G1 becomes noncomposite, the impact on neutral axis is dramatic. When 25% of the girder is noncomposite (D1), very little change is noticed. Once 50% of the girder is noncomposite (D2), the neutral axis jumps by 5.32 inches. As the girder loses composite action the neutral axis of the section moves toward the centroid of the girder. Once the girder becomes completely noncomposite the change is even more obvious increasing 15.22 inches.

Conclusions

This paper presents a numerical analysis, based on a detailed finite element model of an in-service highway bridge, to identify the appropriate damage measures to capture various types of damage likely to occur on the bridge. The bridge used in this study is a simply supported, composite steel girder bridge currently fitted with a long-term continuous monitoring system installed as a part of the joint research efforts of the University of Connecticut and the Connecticut Department of Transportation. Four

damage measures, calculated from measured dynamic strains due to live loads as trucks cross over the bridge, have been identified for the purposes of detecting changes in the structural integrity of the bridge. A finite element model, validated using measured strain data from the actual bridge, is used to model the dynamic response of the bridge due to the loading of a 5-axle truck. Three types of damage are proposed including: fatigue cracking due to truck traffic, impact of a truck passing beneath the bridge, and deterioration of the deck. Five corresponding damage cases are specified to model these damage types: fatigue crack at midpan of G3; fatigue crack at the end of the coverplate of G3; crack initiated by truck impact at the 1/3rd span of G1; noncomposite action of G1, also due to tuck impact; and deterioration of the bridge deck. A detailed analysis of the change in each damage measure due to the five damage cases is conducted and the most sensitive damage measures presented.

The results of the finite element analysis indicate that for this bridge, fatigue cracks at the midspan of a girder are best identified by peak strain, strain distribution, or neutral axis for the damaged girder (G3 for this study). The fatigue crack located at the end of the coverplate is best identified by speak strain for the two girders immediately adjacent to the damaged girder (G2 and G4 for this study) or strain distribution of the damaged girder (G3 for this study). Locating additional sensors at the ends of the coverplates would provide more sensitive measurements and help better identify the damaged girder. The fatigue crack in the exterior girder initiated by impact loading at the 1/3rd span may be identified by peak strain, strain distribution, or neutral axis of the damaged girder. The general conclusion is that the sensitivity of the damage measures to fatigue cracking is dependent on the distance between the damage location and the sensor

location. By placing sensors at or very near the location of damage, the sensitivity of the damage measures is increased and becomes isolated to the damage girder. While midspan and the ends of the coverplates are obvious areas of high stress, placing additional strain sensors in locations where impact loading has occurred is also suggested to monitor the initiation of fatigue cracking at these locations.

Noncomposite behavior between the deck and the girder can be identified using all of the damage measures; however, it is particularly sensitive to the natural frequency and neutral axis damage measures with the neutral axis of the damaged girder being the most sensitive. Therefore, given the unique sensitivity of the natural frequency damage measure, if a change in the peak strain and strain distribution damage measures *as well as* the neutral axis and natural frequency, noncomposite behavior can be identified.

The initiation of bridge deck deterioration is not readily observed by the strain sensors located on the steel girders. Considering the previously discussed damage measures, deck deterioration has been difficult to detect. Of the four damage measures discussed here, neutral axis exhibits the most change, albeit a small change, and is making it the most likely damage measure to indicate problems with the deck.

CHAPTER 3: Quantifying the Level of Observable Damage of an In-Service Long-Term Bridge Monitoring System Deployed on a Composite Steel Girder Bridge

Abstract

A long term bridge monitoring program has been established in Connecticut to monitor critical vulnerabilities in bridges. In doing so it is important to quantify anticipated changes in measurements resulting from different types and levels of damage with the intent of comparing these changes to the inherent variability in actual bridge measurements to determine the minimum level of vulnerability that can be identified through bridge monitoring. This is done in a continuous manner over the life of the bridge. The inherent variability of three specific damage measures including, fundamental natural frequency, strain distribution, and neutral axis location, is determined from actual measured strain measurements. This variability is then used along with a finite element model of the multi-girder composite steel girder bridge to determine the minimum level of damage that is expected to be observable using the current bridge monitoring system.

Introduction

The University of Connecticut and the Connecticut Department of Transportation have been partners in bridge monitoring research for the past twenty years (1-5). Current research efforts focus on the long-term continuous monitoring of six different types of highway bridges located throughout Connecticut (6). The intent of this research is to better understand how to monitor critical vulnerabilities in the State's highway bridges.

Long-term bridge health monitoring can supplement bridge inspections, help to quantify the current structural condition of the bridge, and identify the onset of damage in the structural system (7-8). Continuous monitoring has the potential to identify the presence of damage in a bridge in the early stages before the damage reaches a critical stage or results in the failure of the structure. By examining changes in a bridge's physical characteristics and behavior during operating traffic conditions, using damage measures such as the natural frequency, peak strain, strain distribution, and neutral axis location, it may be possible to determine if damage is present as well as identify the location of the damage. The specific damage measures (DMs), calculated from available bridge response measurements, can be identified for each bridge based on its specific design, use, and critical elements. These DMs can be used to supplement regular visual bridge inspections adding a quantitative measure of the structure's condition. It is important to identify for anticipated damage conditions the most appropriate DMs in a quantitative manner.

In this paper, the composite steel girder bridge and its monitoring system are presented along with the specific DMs identified to best capture the anticipated failure modes of the structure. Actual measured data is used calculate the DMs and identify their unique sensitivities. A finite element model of the bridge is next presented, along with details of the truck loading used in this study. The finite element model is used to determine the minimum level of damage that can be expected to be identified from the various changes in DMs. This information will be used in the SHM system deployed in Connecticut to understand the level of damage expected to be observable.

Composite Steel Girder Bridge and Associated Long-Term Monitoring System

The composite steel girder bridge in this study is a three span, simply supported bridge that carries three lanes of I-91 southbound traffic over the Mattabesset River. The bridge is located near the town of Cromwell, Connecticut. This three lane highway bridge has a total length of 216 feet with two inch expansion joints separating each span. The bridge was built in 1965 and reconstructed in 1998.

Only the first span (Span 1) of the bridge is considered in this study. The girders in Span 1 are W36x194 steel sections with 10"x1" partial length cover plates. The diaphragms are C15x33.9 sections and are located at the quarter points. Figure 1 shows an elevation view and cross section view of the bridge.

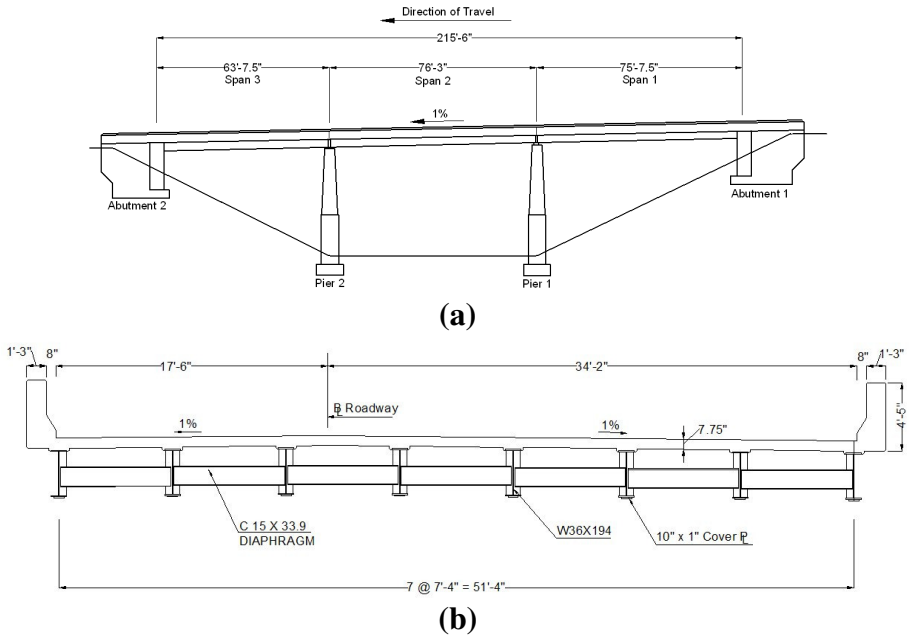

Figure 1. Elevation (a) and Cross Section (b) of the Composite Steel Girder Bridge.

The bridge is currently being monitored by 20 foil-type strain gages attached to the webs of the girders in Spans 1 and 2. A plan view of the bridge including the sensor locations is shown in Figure 2. The sensors are welded on either the top or bottom of the web of the girder. Strain sensors at the bottom of the girder are intended to provide

maximum stress/strain measurements. Collocated strain sensors at the top of the web are used, along with the bottom sensor, to determine the location of the neutral axis of the bridge and identify composite action between the girders and bridge deck.

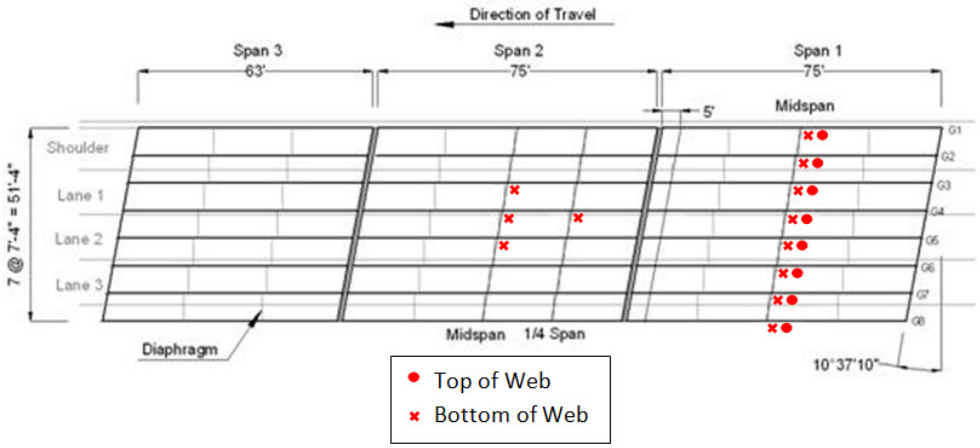

Figure 2. Strain Sensor Locations on the Composite Steel Girder Bridge.

Proposed Damage Measures

Previous research has identified damage measures (DMs) for this composite steel girder bridge (5). This research will examine the effectiveness of three DMs in detecting specific types of damage that are likely to occur on the bridge. The DMs considered include: fundamental natural frequency; strain distribution; and neutral axis location. While environmental and operational variability of bridge structures can affect their dynamic properties and response, it is assumed in this study that any variability is appropriately accounted for, as done by Scianna et al. (9).

The first damage measure is the fundamental natural frequency of the bridge, denoted DM_{ω}. The natural frequency of the bridge is a measure of its dynamic characteristics and is dependent on the physical characteristics of the bridge, namely the mass, stiffness, damping, and the boundary conditions. The presence of damage on the

bridge will change any one of these physical characteristics thus producing a change in the fundamental natural frequency.

The second damage measure is strain distribution for each of the girders, denoted DM_{dist_i}. To determine the strain distribution factor for each girder, the strain distribution at peak strain is used. The strain in each girder is divided by the sum of the strains in all eight girders to determine what percentage of the load a particular girder is carrying. If a girder becomes cracked or otherwise damaged, the strains in the adjacent girders of this indeterminate system will change due to a redistribution of loads.

The last damage measure examined is the location of the neutral axis for each of the girders, denoted DM_{NAi}. Since the location of the neutral axis is dependent on the strain distribution throughout the cross section, including the slab, changes in the location of the neutral axis can be used to identify damage in either the girders or the adjacent slab. Again, measurements taken at the time of the peak strain are used to determine the location of the neutral axis. The strains in the top and bottom of the web are used to calculate the neutral axis location assuming a linear distribution of strain over the height of the cross-section.

Bridge Finite Element Model

In this paper, a finite element model is used to identify the appropriate DMs to use for specific failure modes. The first span, Span 1, of the composite steel girder bridge is modeled using a three-dimensional finite element model, as shown in Figure 3. The span is assumed to be simply supported. This has been validated by field measurements of adjacent spans (i.e. the strain measurements in Span 2 remain unchanged until the truck

on Span 1 enters onto Span 2). The bridge is modeled using plate elements to best capture the local crack behavior and global structural changes. For the undamaged case the model is comprised of 15,952 nodes and 50,348 plate elements. The number of nodes in the damaged models varies slightly from the undamaged case to physically model the different damage cases using more refined plate elements.

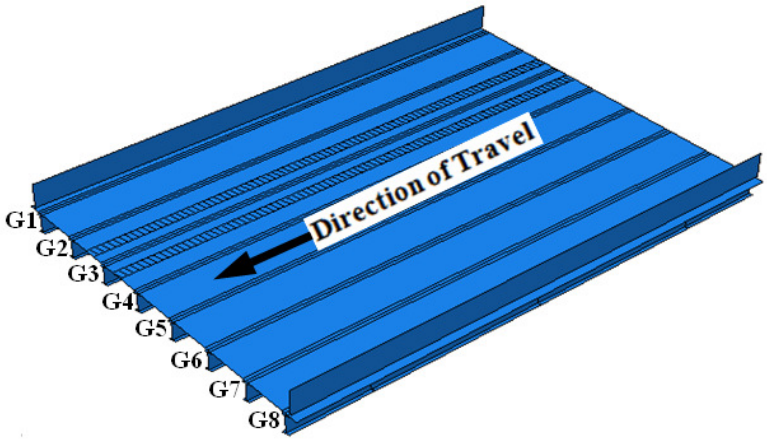

Figure 3. Finite Element Model of Composite Steel Girder Bridge.

The plate elements in the slab and bridge girders were assigned a uniform thickness and material properties, corresponding to the specifications of the composite steel girder bridge. To ensure composite action for the model between the elements in the slab and the elements in the girders, the nodes in the top flanges of the girders were tied to the nodes in the concrete deck. The concrete parapets were modeled by plate elements with a uniform thickness that approximates the weight and dimensions of the actual parapets.

The bridge model is loaded using a five-axle 47ft truck with a 6ft wheelbase and a total weight of 69.76 kips (5). The truck configuration is shown in Figure 4. The truck was positioned so that it straddled Girder 3 to simulate a truck travelling in the right travel lane. The contact area for the tires was based AASHTO specifications and

constitutes a moving area of 10 inches by 20 inches (12). Each axle is modeled as a distributed load over two tire areas. The five axle load pairs of the truck are then incremented over the bridge deck in time corresponding to a vehicle speed of 65 miles per hour (mph). In such a manner the vehicle-bridge dynamic interaction is neglected.

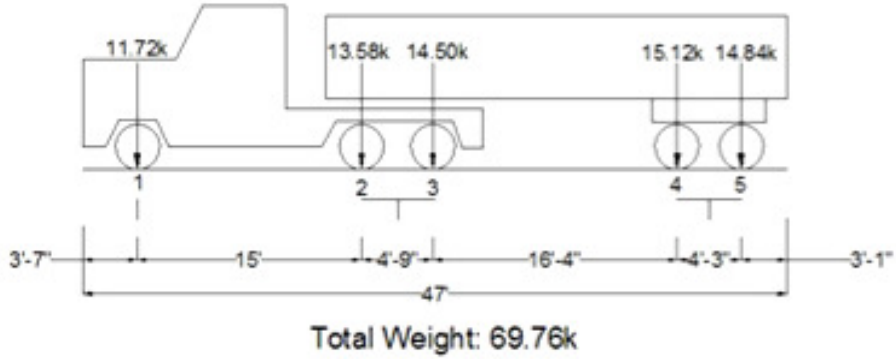

Figure 4. Configuration of Truck Used to Load Bridge.

To verify the finite element model, the response of the undamaged model was compared with measured strain data of a similar truck crossing the bridge (5). Figure 5 shows a comparison of the strain in three of the girders as the truck crosses the bridge. The finite element model yielded peak strains of 55με and 43με in girder 3 (G3) and G4 respectively which corresponds well with the peak strains of 51με and 45με recorded by the monitoring system. The fundamental natural frequencies also match well with 5.14 Hz from the model which fits within the 4.02 and 5.4Hz range calculated from the measured data. Overall, the model is able to capture the dynamic behavior of the bridge loaded by a 5-axle truck.

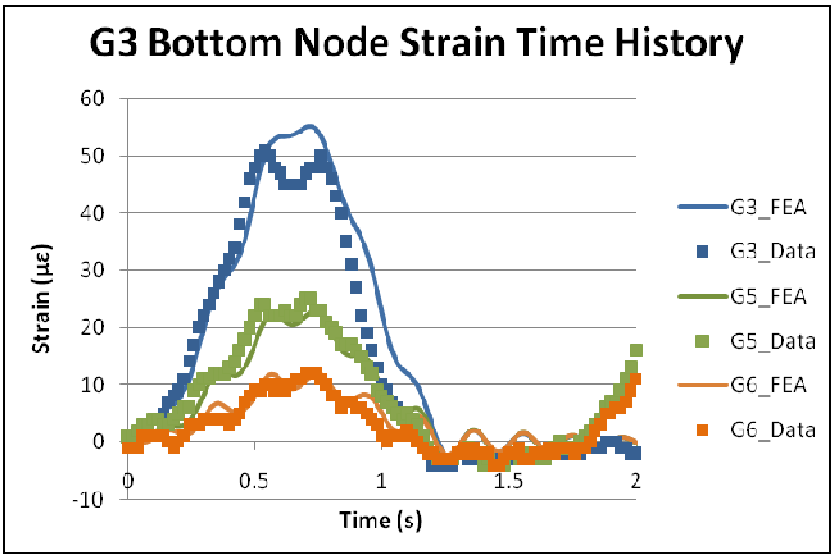

Figure 5. Comparison of Measured and Modeled Bridge Strains.

Uncertainty of Damage Measures

In order to detect damage using the bridge monitoring system, a healthy baseline for the damage measures must be established. This baseline is a random variable due to the presence of measurement noise, variability in loading conditions, and environmental factors. To establish this baseline, data was collected from the bridge over the course of a two hour period. Data was recorded at midday to increase the likelihood of truck traffic over the bridge. By midday, commuter traffic has ebbed and most of the vehicles still on the road are tractor trailers. The data collected during this interval was then processed and broken down into individual truck events and the three damage measures were calculated.

Before the sensitivity of the damage measures can be evaluated, the assumption that the undamaged DMs form a normal distribution must be confirmed. Over the course of two hours of data collection, 228 events were recorded where the peak strain occurred on G3. For each DM, a normal distribution is calculated based on the mean and standard

deviation of the data. The data is then run through a chi-squared goodness of fit test to confirm whether or not that particular damage measure can be reasonably approximated by a normal distribution curve.

Once the assumption of normal distribution is confirmed, the sensitivity of each DM must be quantified. In order to be sure that a data point occurs outside of the normal distribution, the two values that bound 99% of the data were determined. These values occur at $\pm 2.576\sigma$ on either side of the mean.

The first DM, fundamental natural frequency, denoted DM_{ω}, passes the chi-squared goodness of fit test based on a sensitivity value of 0.01. The figure below shows the normal distribution of DM_{ω} along with a histogram of the recorded data. Table 1 shows the change in DM_{ω} required for data to fall outside the healthy distribution of data. As evidenced by this table, there must be a minimum increase or decrease of 0.67Hz in order to detect damage using the natural frequency.

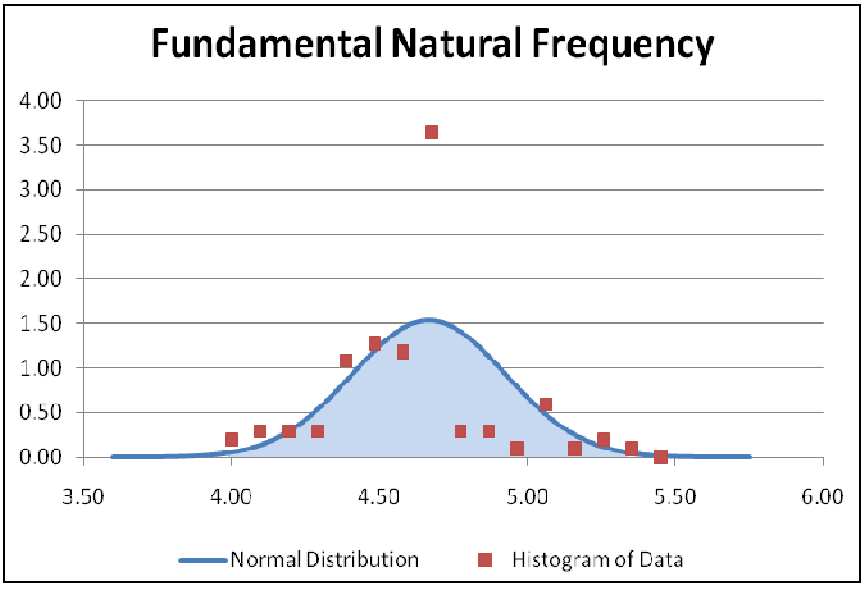

Figure 6. Normal Distribution of DM_{ω}

Table 1. Damage Detection Sensitivity of DM_ω

	DM_ω
Mean	4.667
σ	0.259
Lower Bound	4.000
Upper Bound	5.334
ΔDM (±2.576σ)	±0.67

The second damage measure, strain distribution, is significantly more predictable than the previous damage measures. For this damage measure, all eight girders passed the goodness of fit test at a higher significance level of 0.05. Determining the sensitivity of DM_{dist_i} is a more complex process than determining the sensitivity of DM_ω due to the fact that each girder requires a different ΔDM value in order for damage to be detected on that particular girder. Therefore, each girder must be evaluated individually. While the ΔDM_{dist} for each girder do not appear to be particularly large with a maximum of 6.05% for G5, it is important to look at the change with respect to the mean value. For example, DM_{dist_3} has a mean value of 30.74% and a ΔDM value 5.77% which equates to an 18.8% increase or decrease in DM_{dist_3}. For DM_{dist_8}, the mean value is 0.74% and ΔDM is 1.92%. Since the mean value is so close to zero and a girder cannot carry less than 0% of the load, DM_{dist_8} must increase by 260% for any variation in DM_{dist_8} to be indicative of damage. Such a significant increase on a girder that carries a minimal amount of the load is unlikely particularly since the load distribution to a damaged girder tends to drop as the severity of the damage increases, thus DM_{dist_8} is rendered ineffective. Examining each DM_{dist} in this fashion shows that the sensitivity of the damage measure increases as the percentage of load carried by the girder increases and that DM_{dist_6} through DM_{dist_8} have such low sensitivities, they are likely not usable as damage measures.

Table 2. Damage Detection Sensitivity of Strain Distribution

	DM_{dist_1}	DM_{dist_2}	DM_{dist_3}	DM_{dist_4}	DM_{dist_5}	DM_{dist_6}	DM_{dist_7}	DM_{dist_8}
Mean	5.66%	16.31%	30.74%	27.16%	12.41%	5.21%	1.76%	0.74%
σ	1.14%	1.78%	2.24%	2.07%	2.35%	1.69%	1.30%	0.75%
Lower Bound	2.73%	11.72%	24.97%	21.84%	6.36%	0.84%	-1.59%	-1.18%
Upper Bound	8.60%	20.91%	36.52%	32.48%	18.46%	9.57%	5.12%	2.66%
ΔDM (±2.576σ)	±2.93%	±4.59%	±5.77%	±5.32%	±6.05%	±4.37%	±3.36%	±1.92%

Determining the effectiveness of the last damage measure, neutral axis, is more complicated due to the fact that not all of the girders passed the goodness of fit test. Table 3 shows the p-values for all eight girders. Unlike strain distribution where all of the girders passed, neutral axis has three girders that pass and five that do not. The girders that pass show varying degrees of goodness of fit. G2 has by far the best fit with a p-value of 0.8925 while G3 has the lowest with 0.0638 coming in just over the cutoff value of 0.05.

Table 3. P-Values for the Neutral Axis Damage Measures

Girder	Probability
G1	8.0728x10-9
G2	***0.8925***
G3	***0.0638***
G4	***0.1331***
G5	6.6x10-8
G6	4.0773x-9
G7	1.6261x-8
G8	0.0012

Examination of the sensitivity of DM_{NA} for G2, G3, and G4, shows that of the three DMs discussed here, DM_{NA} has the highest sensitivity to damage. The changed required for DM_{NA} to detect damage is small in comparison with the expected mean value for the neutral axis of each girder. G3 is the least sensitive of the three but still requires a change of 1.47 inches which equates to a 13.3% change in the location of the

neutral axis. The other difference between neutral axis and the other damage measures is that the sensitivity is relatively consistent across the three girders. In strain distribution, G3 has the highest sensitivity with sensitivity decreasing significantly as the load on the girder decreases. For DM_{NA}, the three usable girders have fairly equal sensitivity.

Table 4. Damage Detection Sensitivity of Neutral Axis

	DM_{NA2}	DM_{NA3}	DM_{NA4}
Mean	12.65”	11.07”	10.84”
σ	0.59”	0.57”	0.40”
Lower Bound	11.14”	9.60”	9.80”
Upper Bound	14.17”	12.54”	11.87”
ΔDM (±2.576σ)	±1.52”	±1.47”	±1.04”

Bridge Damage

There are many different types of damage a composite steel girder bridge might experience. For this paper, two types of damage are considered: fatigue cracking due to truck traffic and impact of a truck passing under the bridge. In order to cover these potential damage scenarios, four different cases are considered.

Cases 1 and 2 represent fatigue related damage to the bridge. Cases 3 and 4 capture potential damage as the result of a truck impacting the exterior girder of the bridge.

Case 1- Cracking in Girder 3 at Midspan: The first damage case was chosen to represent a fatigue crack developing in the area of highest stress on the bridge, the midspan. In this case, the damage is located directly beneath the strain gage which means the damage should be easily detectable even during the early stages of crack development.

Case 2- Cracking in Girder 3 at the End of the Coverplate: The second damage case is representative of a fatigue crack that develops as the result of the discontinuity and stress concentration caused by the end of the partial length coverplate.

Case 3- Cracking in Girder 1 at 1/3rd Span: The third damage case is the first of two designed to simulate damage as the result of a truck impacting the exterior girder. As the result of the impact, damage is introduced to the girder as a crack that will develop slowly over time following the impact event. The crack was placed at 1/3rd span, directly over the slow lane of a roadway travelling under the bridge, to model the location most likely to be susceptible to impact. The location of damage for these first three cases is shown on the finite model in Figure 7.

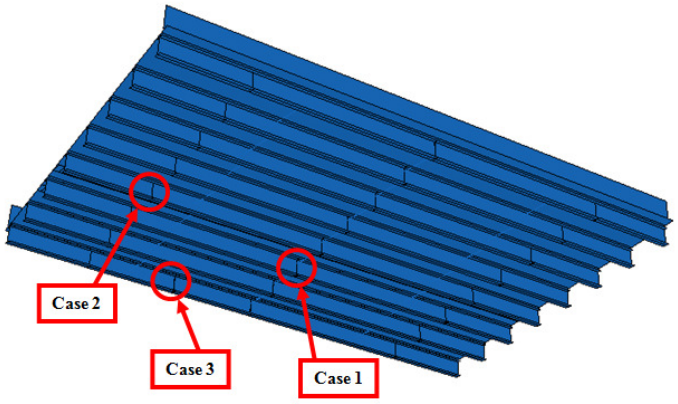

Figure 7. Damage Location for Cases 1, 2, & 3.

For damage cases 1 through 3 where cracking of the girder is involved, a total of four levels of damage were used to model the progression of a 3/8 inch wide crack, as in Farrar et al. (11). Figure 8 shows a drawing of the cross-section of the G3 girder for all four damage levels.

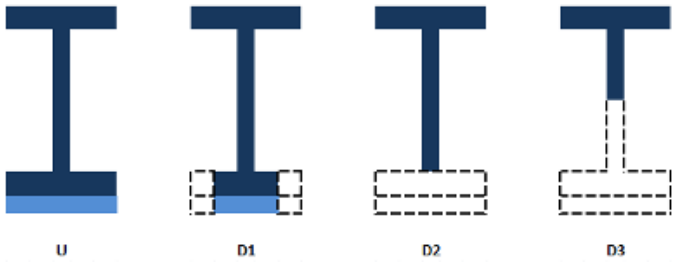

Figure 8. Cross-Section of Damaged Bridge Girder at Damage Location: undamaged (U): 50% reduction in the bottom flange and cover plate (D1): 100% reduction in the bottom flange and cover plate (D2): and 100% reduction in the bottom flange and cover plate and 50% reduction of the web (D3).

Case 4- Loss of Composite Action in Girder: In addition to potential cracking in the exterior girder as the result of a truck impact, it is possible that the girder may become noncomposite as the result of the large horizontal force applied. Three levels of noncomposite action are modeled: one quarter of the girder centered on the impact site at 1/3rd span becomes noncomposite (D1); the half of the girder closest to the impact site becomes noncomposite (D2); and the entire Girder 1 becomes noncomposite (D3).

Results

In order to detect damage on the actual composite steel girder bridge, data collected from the bridge will be compared with a healthy normal distribution of a damage measure. To judge the degree of damage that can be detected by the system, the healthy distributions calculated from 2-hours of data collection were examined to determine what change would be required to produce data points outside the healthy range of data. This is then compared with the changes in the DMs observed using the results of the finite element model to determine what level of damage is detectable.

In a previous study (12), the changes in the damage measures due to the four damage cases were quantified and evaluated to determine which DMs were most

effective for identifying each type of damage. For a fatigue crack at the midspan of a girder (Case 1) and for a fatigue crack at 1/3rd span of an exterior girder initiated by truck impact (Case 3), strain DM_{dist} and DM_{NA} were identified as the most effective damage measures. For a fatigue crack at the end of the coverplate, DM_{dist} was the most effective damage measure. Noncomposite behavior was able to be detected by all three damage measures: DM_{ω}; DM_{dist}; and DM_{NA}.

For the three damage cases involving fatigue cracking, the ability of DM_{dist} to detect damage depends heavily on the damage location's proximity to the sensor. Where the damage occurs at midspan, the initial change in DM_{dist_3} of 3.64% is not large enough to be detected given the minimum required change of 5.39% for G3. However, once the crack has progressed through 100% of the flange (D2) the anticipated change in DM_{dist_3} rises sharply to 25.72% well above the sensitivity range for that particular damage measure. In the other cases involving fatigue cracks, the changes in DM_{dist} do not exceed the sensitivity range of their respective girders (G2 for cracking at the end of the cover plate and G1 for cracking at the 1/3rd span of G1) even for the most severe damage.

In addition to the distance between the damage and the sensor, the girder that the damage occurs on also figures heavily into the ability to detect damage. As noted earlier, the sensitivity of DM_{dist} decreases for the less heavily loaded girders which means damage even at midspan on G7 or G8 could be very difficult to detect. Since the distribution load on these girders is small (averaging 1.76% for G7 and 0.74% for G8), the load on these girders would have to increase significantly to produce a ΔDM_{dist} large enough to be indicative of damage.

The neutral axis damage measure is similarly affected by proximity of the damage to the sensor and to the location of the damaged girder. DM_{NA} was identified as a damage measure useful for detecting fatigue cracks at midspan or at 1/3rd span of an exterior girder; however, since DM_{NA1} and DM_{NA8} did not follow normal distributions, fatigue cracks due to truck impacts on an exterior girder are not detectable using this DM. Neutral axis can still be used to detect damage at midspan although there are limitations. DM_{NA} can only be used to find midspan cracks on G2, G3, or G4 and the changes observed in the finite element model for cracking at midpan of G3 showed changes of 0.46, 1.17, and 28.63 inches for the three damage levels. The highest level of damage clearly exceeds the sensitivity of DM_{NA3} and the second damage level, where 100% of the flange has cracked falls just short of the sensitivity range which would indicate that damage may be detectible just after the crack has begun to progress into the web.

Noncomposite behavior is unique in that all three damage measures have been identified as having the potential for detecting this type of damage. Although DM_{ω} passes the goodness of fit test with a lower significance level than DM_{dist} and DM_{NA}, the required change is relatively small, only 0.6 to 0.73Hz. In the finite element model, as G1 becomes behaves progressively more noncomposite with the deck, the fundamental natural frequency changes by 0.85Hz (D2) and 1.88Hz thus exceeding the sensitivity level of DM_{ω}. The sensitivity DM_{dist_1} is also exceeded for noncomposite behavior but only for the highest level of damage, a fully noncomposite girder. DM_{NA1} was eliminated as a viable damage measure and therefore cannot be used to confirm noncomposite behavior. However, the presence of significant changes in both DM_{ω} and DM_{dist} is unique to this particular type of damage and can be used in conjunction with one another

to identify noncomposite behavior. Although DM_{dist_8} and DM_{NA8} have been shown to be either ineffective or unusable, DM_{ω} still remains a viable damage measure indicating that noncomposite behavior of either exterior girder is potentially detectable despite the limitations of the damage measures on these girders.

Conclusions

This paper examined three different damage detection measures using a finite element model of a simply supported, steel girder composite bridge currently being monitored by the University of Connecticut and the Connecticut Department of Transportation. By modeling the first span of the Cromwell Bridge and introducing damage in critical locations, the changes in the damage measures as the result of varying degrees of damage can be determined. Comparing the changes observed in the damage measures using the finite element model and the actual variability of damage measures collected from the Cromwell Bridge, it is possible to quantify the minimum level of damage that is expected to be observable using the different damage measure for this bridge.

Of the three damage measures, strain distribution demonstrates the most predictable behavior as all eight girders were found to follow a normal distribution. DM_{dist} has a widely varying sensitivity with the more heavily loaded girders having the highest sensitivity. Although it was found that G7 and G8 would not be able to detect damage due to their very low sensitivity, these two girders carry a very minimal percentage of the load on the bridge (1.76% and 0.74% respectively) and would require an increase in DM_{dist} in order to produce a data outside the healthy baseline. Since G7

carries the outer edge of the left travel lane where no trucks have been observed and G8 carries the shoulder and parapet, load increases in these girders is unlikely. The sensitivities of the most load bearing girders are high enough that damage is detectable when located in close proximity to a strain sensor. The location of the damage in relation to the sensor and the girder on which the damage occurs is critical to strain distribution's effectiveness as a damage measure. In order to detect damage, the sensor must be located within a short distance of the damage as evidenced by the fact that damage can be detected for a fatigue crack at midspan but not at the end of the coverplate or at the 1/3rd span.

Natural frequency and neutral axis both show potential for damage detection. This particular measure is useful in situations where large changes in natural frequency are anticipated as was the case when G1 became noncomposite. There were not sufficiently large enough changes in the fundamental natural frequency for DM_{ω} to be useful for detecting any type of cracking in the girders.

Neutral axis has the highest sensitivity and therefore the best potential for detecting damage. Only, the three most heavily loaded girders are found to follow a normal distribution. Like strain distribution, neutral axis is extremely sensitive to the damage location requiring that the damage be located in close proximity to the sensor. In the case where the crack and the sensor were collocated, neutral axis can detect damage once the crack has begun to advance into the web of the girder. The ability DM_{NA} to detect damage is somewhat limited by the fact that only three girders can be used; however, the larger loads are carried by the three viable girders which produces the largest changes in stress therefore increasing the likelihood of crack development.

Throughout this discussion there has been a common theme. While there is potential to detect damage using the damage measures discussed here, damage in a composite steel girder bridge is more difficult to detect when it is not located near a sensor. Since it is both costly and unrealistic to develop a system where damage would develop within a few feet of a sensor at any point on a bridge, it is important to identify critical locations that are most likely to be susceptible to damage such as the midspan or ends of the coverplates. Placing additional sensors in locations where impact loading has occurred is also suggested to monitor the initiation of fatigue cracking due to truck impact.

Acknowledgements

The authors gratefully acknowledge the Federal Highway Administration and the Connecticut Department of Transportation for funding of this project through the State Planning and Research (SPR) program, project SPR 2256. The authors would like to express our gratitude for outstanding work by Connecticut Department of Transportation employees to make this work possible. This report, prepared in cooperation with the Connecticut Department of Transportation and the Federal Highway Administration, does not constitute a standard, specification, or regulation. The contents of this report reflect the views of the authors who are responsible for the facts and the accuracy of the data herein. The contents do not necessarily reflect the views of the Connecticut Department of Transportation or the Federal Highway Administration. The U.S. Government and the Connecticut Department of Transportation do not endorse products or manufacturers.

REFERENCES

1. A.J. Cardini and J.T. DeWolf. Long-term Structural Health Monitoring of a Multi-girder Steel Composite Bridge Using Strain Data. Journal of Structural Health Monitoring, Vol. 8, No. 1:47-58. 2009.

2. J.T. DeWolf, A.J. Cardini, J.K. Olund and P. F. D'Attilio. Structural Health Monitoring of Three Bridges in Connecticut. Annual Meeting of Transportation Research Board, Washington, D.C., 17 pages. 2009.

3. J.T. DeWolf and M. P. Culmo. History of Connecticut's Short-Term Strain Monitoring Program for Evaluation of Steel Bridges. Annual Meeting of Transportation Research Board, Washington, D.C., 16 pages. 2009.

4. J.T. DeWolf. History of Connecticut's Short-Term Strain Program for Evaluation of Steel Bridges. Report No. CT-2251-F-09-6, Connecticut Department of Transportation. 2009.

5. A.J. Cardini and J. T. DeWolf. Implementation of a Long-Term Bridge Weigh-In-Motion System for a Steel Girder Bridge in the Interstate Highway System. Journal of Bridge Engineering, American Society of Civil Engineers, Vol. 14, No. 6:418-423. 2009.

6. J.K. Olund and J.T. DeWolf. Passive Structural Health Monitoring of Connecticut's Bridge Infrastructure. Journal of Infrastructure Systems, American Society of Civil Engineers. Vol. 13, No. 4:330-339. 2007.

7. Doebling SW, Farrar CR, Prime MB. A summary review of vibration-based damage identification methods. The Shock and Vibration Digest; 30(2): 91-105. 1998.

8. Carden EP, Fanning P. Vibration based condition monitoring: a review. International Journal of Structural Health Monitoring; 3(4): 355-377. International Journal of Structural Health Monitoring 2004; 3(4): 355-377. 2004.

9. Scianna, A. and Christenson, R. "Probabilistic Structural Health Monitoring Method Applied to the Bridge Health Monitoring Benchmark Problem." *Transportation Research Record: Journal of the Transportation Research Board*, Volume 2131. 2009.

10. "3.6.1.2.5 Tire Contact Area." *AASHTO LRFD Bridge Design Specifications: Customary U.S. Units, 4th Ed*. American Association of State Highway and Transportation Officials. 2007

11. Farrar, C.R. and Jauregui, D.A. "Comparative Study of Damage Identification Algorithms Applied to a Bridge: I. Experiment." *Smart Materials and Structures*, Volume 7, Number 5, 704-719. 1997.

12. Gucunski, N et al. “Multiple Complementary Nondestructive Evaluation Technologies for Condition Assessment of Concrete Bridge Decks.” *Transportation Research Record: Journal of the Transportation Research Board*, Volume 2201. 2010.

13. Gucunski, N et al. “Impact Echo Data from Bridge Deck Testing: Visualization and Interpretation.” *Transportation Research Record: Journal of the Transportation Research Board*, Volume 2050. 2008.

14. Bendat, J.S. and Piersol, A.G. *Random Data Analysis and Measurement Procedures,* Third Edition. Wiley Series in Probability and Statistics, New York, 2000.

15. Lauzon R, DeWolf JT. “Ambient vibration monitoring of a highway bridge undergoing a destructive test”. ASCE Journal of Bridge Engineering; 11(5): 602-610. 2006.

APPENDIX A- Finite Element Model ABAQUS Manual

Introduction

This manual contains all of the specifications and procedures that were used to build and analyze the finite element model of the Cromwell Bridge. Part 1 provides all of the dimensions and specifications as well as the process used to build the model. It also discusses model mesh and the element types used. The methods used to analyse the model and process the data are presented in Part 3.

Part 1- Building the Finite Element Model

Bridge Geometry

The figures below show the dimensions of the Cromwell Bridge. Only Span 1 was modeled for the purposes of this research. To simplify the model, the slope of the bridge and the crown of the road surface were ignored.

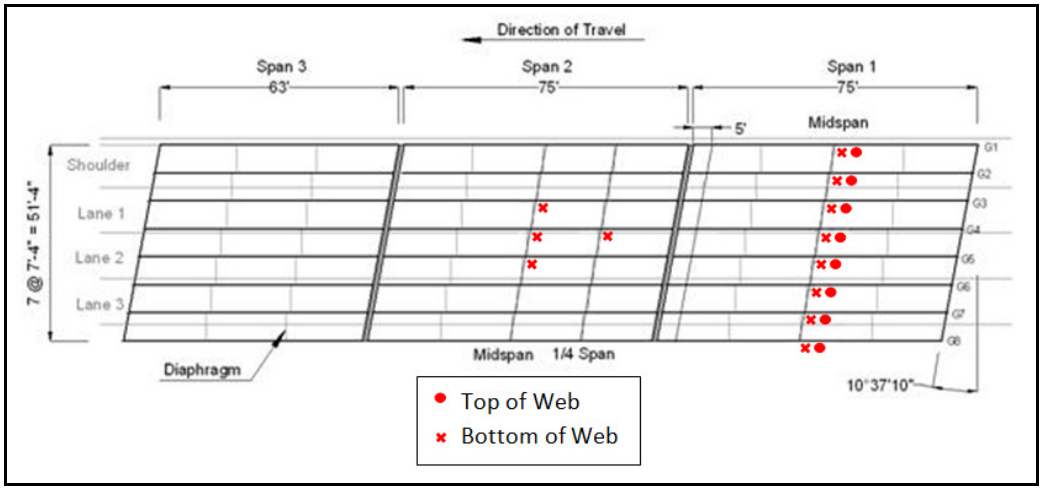

Figure 1. Plan View

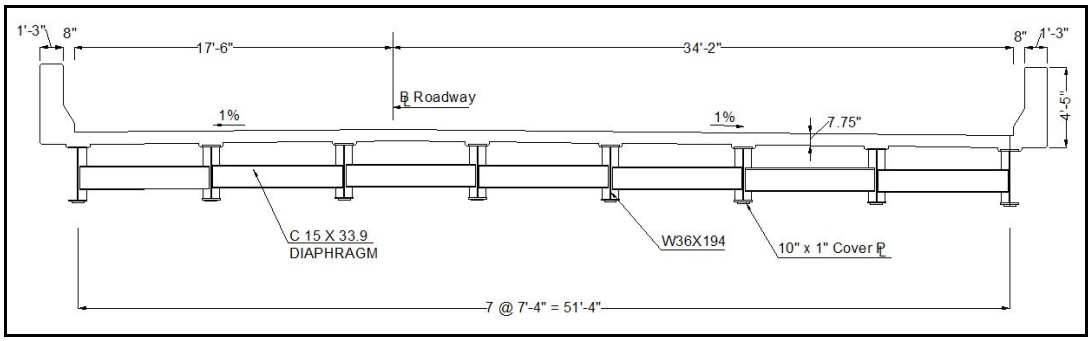

Figure 2. Cross Section View

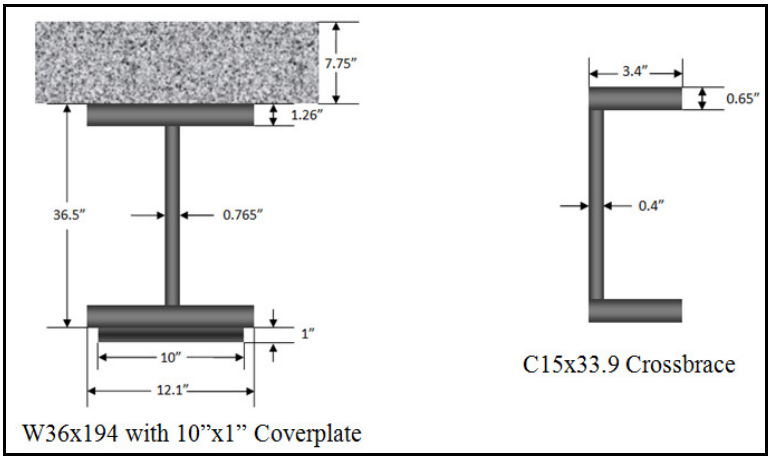

Figure 3. Member Dimensions

Material Specifications

The girders and cross-braces are all assumed to be made from the same steel. The concrete deck was assumed to be 4000psi strength. The material properties of the materials used are listed below:

Table 1. Steel Material Properties

Property	**Value**
Modulus of Elasticity (E)	29000 ksi
Poisson's Ratio	0.3
Density	7.349×10^{-7} kip·s^2/in^4

Table 2. Concrete Material Properties

Property	**Value**
Modulus of Elasticity (E)	626400 ksi
Poisson's Ratio	0.2
Density	4.662729×10^{-3} kip·s^2/in^4

It is important to note that when using American or English units in ABAQUS the density must be in terms of mass (lbm) not weight (lbf). To ensure compatibility with the other material properties, the densities of the two materials were calculated using the following method:

$$0.284\frac{lb}{in^3}\times\frac{1}{1000}\frac{kip}{lb}\times\frac{1}{386.4}\frac{s^2}{in}=7.349\times10^{-7}\frac{kip\cdot s^2}{in^4}$$

where 386.4 in/s^2 (32.2 ft/s^2) is the acceleration due to gravity.

The figures below show how these values are entered into ABAQUS/CAE. Note that there are no units given for any of the property values. The user must keep track of these values to ensure that they are compatible with each other as well as the geometry of the model. The bridge geometry was drafted in inches so that the girder cross-sectional dimensions could be modeled accurately; therefore, the material properties are also given in terms of inches.

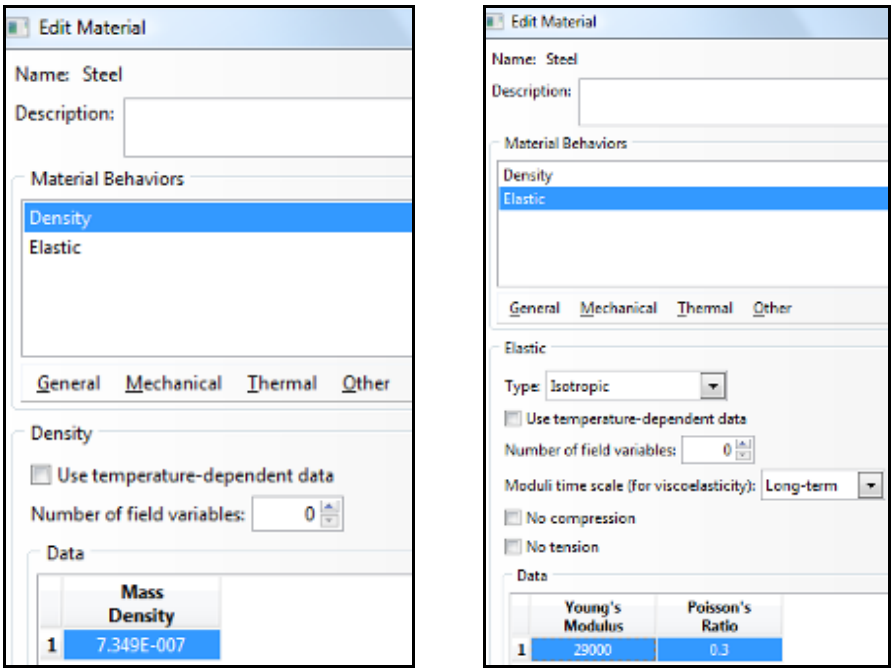

Figure 4. Material Property Entry in ABAQUS/CAE

Creating the Parts

Prior to building this model it was determined that shell elements would be used since shell elements are able to capture local crack behavior in addition to global structural changes. The first step in creating a shell element is establishing the datam or the plane in which the part is drawn. The figure below shows the datum for each of the components involved in modeling a girder. With a total girder depth of 36.5 inches and flange thicknesses of 1.26 inches, the centerlines of the flanges are 35.24 inches from one another and therefore the two datums are spaced at this same distance. The web datum is then positioned perpendicular to these two datums so that it intersects them along their centerlines.

In order to model the partial length coverplates, rather than model the coverplates as a separate plate element from the flange, the center 51ft of the girder was modeled using a cross section equivalent to a W36x194 beam with an increased bottome flange thickness. This method was selected based on a previous model of the Cromwell Bridge and helped to simplify the process used to model cracking in a girder by reducing the number of parts that had to be modified or partitioned. Two additonal datums are necessary for the modified web and bottom flange sections producing a total of five parts to form each girder.

The datums used to create each girder component are repeated for each of the eight girders with each set of datums offset along the x-direction to correspond to the spacing between the girders. Once the girders are modeled, the deck and parapets are modeled using the same procedure. It is important to be sure that the top flanges, deck, and parapets are offset the approprate distance to accommodate the thickness of each of

the components. The datums for the top flanges are positioned 4.505" below the deck, and the parapets are offset 3.875" above the deck. Figure 6 shows the arrangement of these parts. Once a datum is established, the part can be drawn and the material and thickness assigned. A total of 43 parts were created using this procedure.

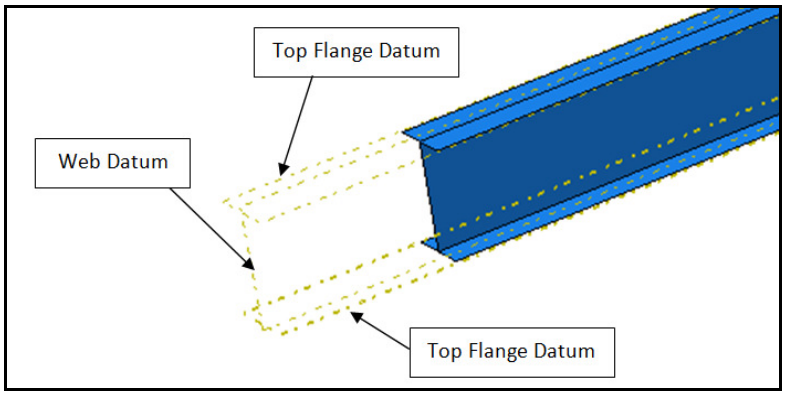

Figure 5. Part Datums

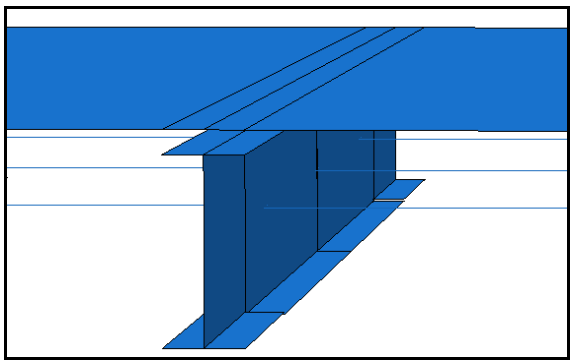

Figure 6. Arrangement of the Plate and Beam Elements for a Typical Cross-Section

The crossbraces were modeled using beam elements. Modeling the crossbraces as beams greatly simplified the assembly of the model. The use of plates or solid elements requires extensive partitioning in order to ensure mesh combatibility between the components. For example, the deck was partitioned along the lengths of the girders to ensure that the number of elements in the deck is equal to the number of elements in the top flanges of the girders. Mesh incompatibility would result in inaccuracies in the model. Another reason beam elements were used was that the stresses and strains in the

crossbraces were not examined in this research. Modeling the crossbraces as plates would have added a large number of unnecessary elements and nodes thereby increasing computation time.

As was the case with the shell elements, a datum is created to draw the crossbrace. Since three crossbraces are located between the girders, the datums are offset along the length (z-axis) and width (x-axis) of the bridge. The first set of crossbraces is positioned 19'-6" from the northern end of the bridge. The next two sets of cross braces are equally spaced at 18'-9".

Assembling the Model

Once the parts making up the girders and crossbraces were modeled, they were all assembled to create one part labeled "Superstructure". A total of 61 parts were used to model the superstructure of the bridge, assembling them under one part greatly simplified the process of editing the model.

By assembling these components as one part, the material properties, mesh, and constraints (rigid ties) can all by controlled and modified within that one part rather than referring back to each part individually. This was particularly important for the development of the model mesh. Meshing the substructure as a whole made it easier to ensure that each girder was meshed the same and that the mesh was free of significant distortion. Meshing the parts individually would have been time consuming and difficult to ensure compatibility.

The deck and parapets are added to the assembly individually. Since they do not come in direct contact with the substructure or each other, the parts cannot be merged as

was the case with the substructure and therefore they must be attached to one another using rigid ties.

These ties are applied at a number of locations throughout the model. The top flanges are tied to the underside of the deck, the parapets are ties to the top side of the deck, and the crossbraces are tied to the webs of the girders. To be sure that the ties do not conflict with one another, the deck was selected as the master surface for all ties involving the deck. If the deck were to be selected as the slave surface, an error would arise since the deck cannot be a slave surface to multiple constraints. The same concept was applied when assigning the ties for the crossbraces. The web was always selected as the master surface and the node at the end of the crossbrace was selected as the slave surface.

Assigning Properties and Materials

While the material and section properties may be assigned to each part before they are assembled, it was found to be easier to manage the material properties by assigning them to the substructure part that was created by merging the assembly. This meant that material properties could be changed without having to reassemble the model.

For the shell elements, the properties are easily assigned by selecting the element and the appropriate section definition. A section definition specifies both the material type and element thickness. A section definition was created for the flanges, web, deck, and parapets. The parapets were modeled using a thickness roughly equivalent to the weight of the actual cross section.

For the beam elements, a beam cross-section, material, and beam orientation must be assigned. The beam orientation is important to ensure that the cross-section of the beam is positioned correctly. The figure below shows the beam orientation and the resulting 3D rendering of a crossbrace.

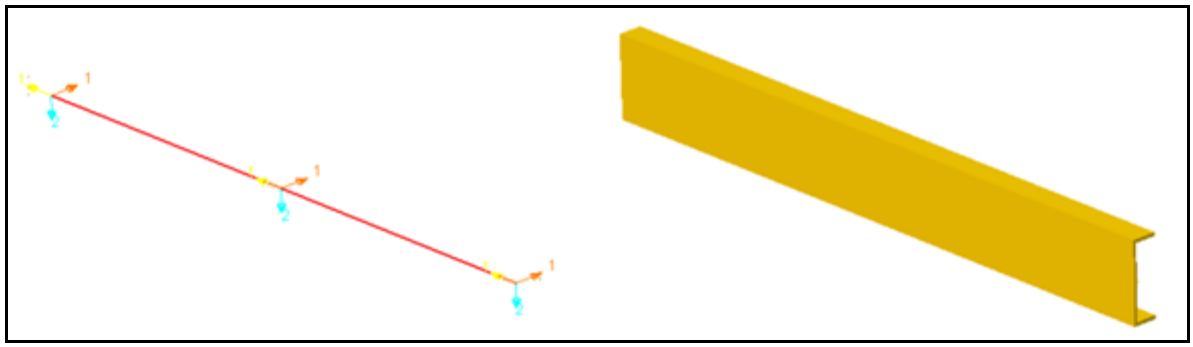

Figure 7. Beam Cross-Section Orientation

Partitioning

As discussed in the previous sections, partitioning is necessary to develop a good mesh. It is also used to model the dynamic truck loading and to deliniate the sensor locations on the model. The figures below show the partitioning of the deck and the girders.

Figure 8 shows the partitioning of the deck. The partitions for the girders were created for the purposes of ensuring mesh compatibility as well as providing a surface for the rigid ties between the girders and the deck. The deck was also partitioned into 10”x20” areas along the length of the bridge. Each of these areas represents the contact area of the truck tires. The wheel loads were modeled as distributed loads over these areas. For a more detailed description of the process used to model the truck load, refer to Appendix B.

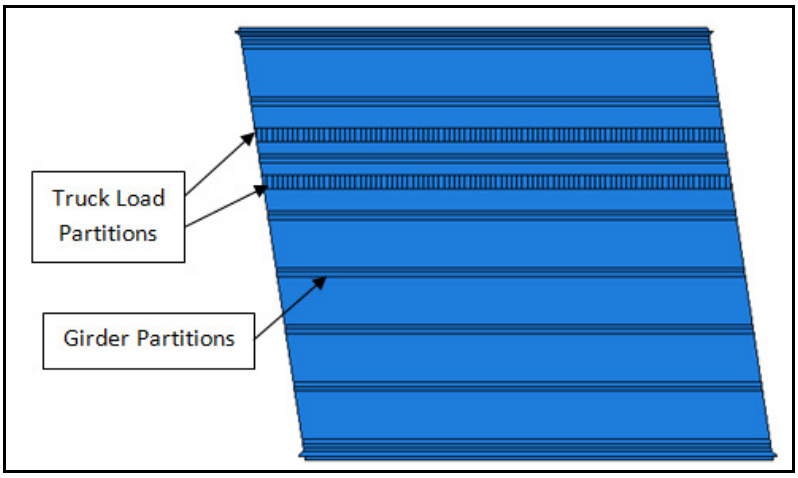

Figure 8. Deck Partitioning

The partitioning of the girders was necessary for both modeling a crack in the girder and to delineate the sensor locations. A 5/8" wide crack was modeled for all cases involving a fatigue crack in a girder. This strip was partitioned through the cross-section of the girder wherever the crack was being modeled. The partitions helped to control the mesh in these areas since discontinuities in the structure as the result of the crack made controling the quality of the mesh difficult. Being able to assign the number of elements along these partitions helps to keep the number of elements through the web and flange consistent across the length of the girder.

The 5/8" strip that was used to partition the fatigue crack was also used to partition the sensor locations. Since the initial damage case investigated was a fatigue crack at midspan on girder three, using the same partition for both the damage and the sensors simiplified the partitioning process. For the sensors, additional partitions were added to delineate the sensors. As shown in Figure 8, two small squares 5/8"x5/8" were created 2" away from the flanges in the same location as the sensors on the bridge. These two squares represent the top and bottom node sensors for the model.

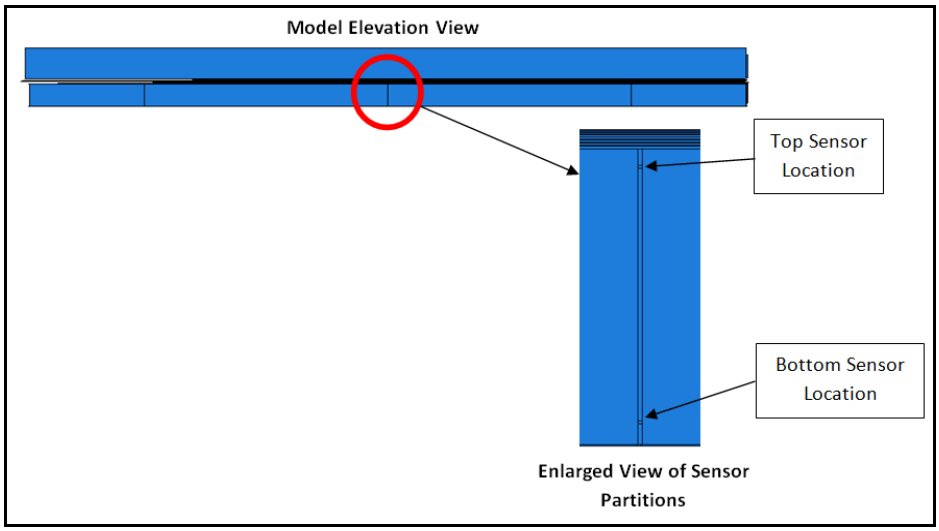

Figure 9. Girder Partitioning

To use these partitions as sensors, a set was created. A set is a specific selection of nodes, surfaces, or elements selected by the user. For each of the eight girders these squares were selected individually and labeled as the top or bottom node for a particular girder (i.e. G1_top, G1_bottom, etc.). This produced a total of 16 sets. The sensors were selected individually to ease the idenification of data during post-processing.

It is important to note that the sensors sets must be plates rather than nodes in order for ABAQUS to calculate strain. If a single node is selected as the sensor, displacements or accelerations may be obtained, but the program will not compute strains even if this output is requested. Modeling the sensor as a very small shell element, ensures that the strains calculated by the program are as close as possible to the data collected by the sensors in the field.

Element Types

Before the model can be meshed, the parts must all be assigned element types and mesh controls. The girders, coverplates, bridge deck, and parapets were all modeled using

S8R elements. S8R elements are quadratic shell elements with reduced integration. The crossbraces were modeled using quadratic B32 elements.

Figures 10 and 11 show the mesh controls that were applied to all of the shell elements and the resulting mesh of the finite element model. These controls ensured that the mesh did not become distorted and helped to avoid errors when running the model. As evidenced by the second figure, despite the number of parts being meshed the mesh has minimal distortion which improves the results of the analysis.

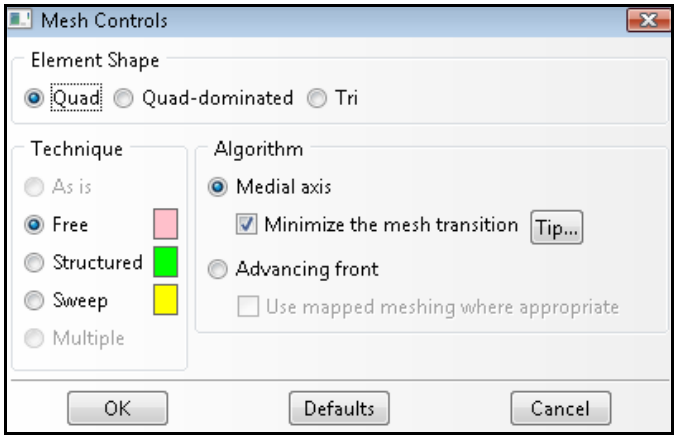

Figure 10. Mesh Controls

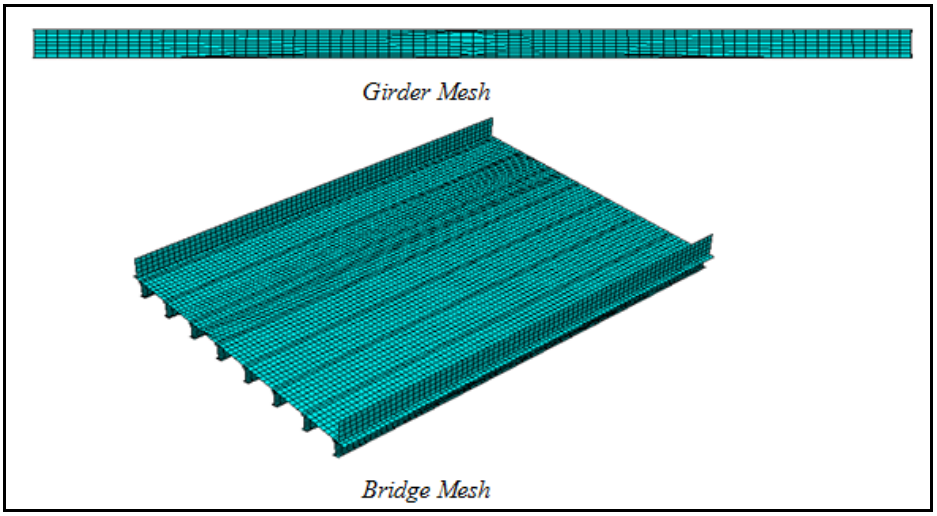

Figure 11. Finite Element Model Mesh

Part 3- Analysing and Post-Processing

Analysis Steps

In order to perform a dynamic analysis of the structure, two steps are required. The first is the frequency analysis which is performed using the "Frequency" step from the "Dynamic Analysis" category. In this step, the user identifies the number of frequencies to be calculated. Since the damping of this model is to be based on modal damping, a total of 80 frequencies were requested. This quantity can be changed by editing the step.

The second step is the dynamic analysis of the truck crossing the bridge. This is performed by the "Modal Dynamics" step which also falls under the "Dynamic Analysis" category. The "Frequency" step must precede this one since the "Modal Dynamics" step uses the frequencies calculated that step. In the "Modal Dynamics" step, the method of damping is selected. For this research, modal damping was selected with 5% damping applied to all 80 natural frequencies.

In this step, the length of the analysis is also specified as well as the time increments. To capture the complete response of the bridge due to the truck crossing, a total analysis time of 5 seconds was selected with an increment of 0.001 seconds.

Selecting the Output Values

Two different types of outputs were used in this research: Field Output and History Output. A Field Output request is made when the response is not time dependent, as is the case with natural frequency, producing a single value for each of the

selected sets. For the mode shapes, the entire model is selected as the set and the desired variable is displacement. These can be identified by creating a Field Output request.

To determine the response of the bridge due to the truck loading, a History Output is needed. This output provides a time history of the selected variables for the sets identified. In this case, the 16 sensor sets are selected and the desired variable is strain. Particularly for time histories where there may be thousands of data points for each node, creating a set for the particular points or elements that are being examined helps to significantly reduce computation time in addition to drastically simplifying the post-processing of the data.

Post-Processing the Data

Once the finite element model has been analyzed, the next step is to examine the outputs requested. The mode shapes and natural frequencies are easily obtained by going to the Results menu and selecting Field Output. From this menu, the user can select the variable to be displayed by model as well as the step the user wishes to view. For the natural frequency, displacement should be selected. The natural frequencies and mode shapes can be examined simultaneously in the user interface or the complete list of natural frequencies can also be viewed by returning to the Field Output screen previously mentioned and selecting “Step”.

The strain data must be processed a little further before it can be used to calculate the damage measures. To access the strain data, a data file must be created for each sensor. To do this, select XY Data and create a new file. The figure below shows the

options available when creating an XY Data file. Since History Outputs were requested while building the model, "ODB history output" must be selected as the data source.

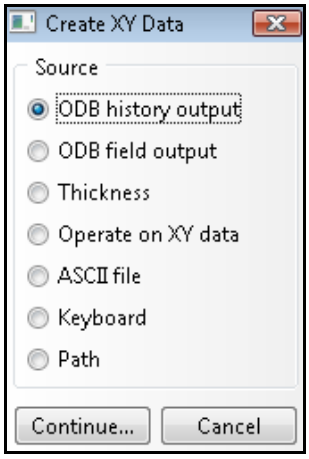

Figure 12. XY Data Source Selection

Once ODB History Output is selected, all of the outputs that were identified previously are available for selection. Since the sensors were created using a small portion of a shell element, there are a total of eight strains calculated per sensor. These strains are calculated on the four corners of the element on both sides of the element. To obtain a single strain value for each sensor, all eight strains for that particular sensor are selected as shown in Figure 13. The strains are easily identifiable since the sensors were selected as individual sets. Had all 16 sensors been selected as one set, all of the requested outputs would have been labeled under the set name and the user would have to determine which sensor was represented by which element number. Labeling each sensor individually makes processing the data much simpler and ensures that the each time history is associated with the correct sensor.

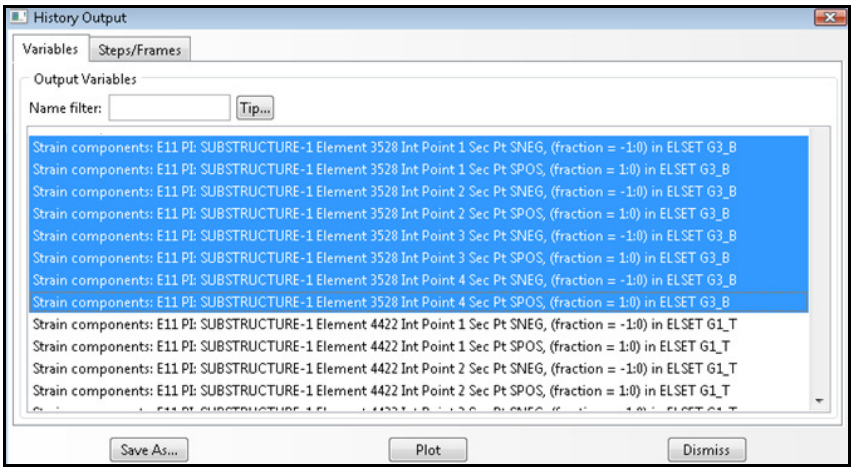

Figure 13. Selecting the XY Data

Once the eight strains for a particular sensor are selected, the data must be saved as an average of the outputs selected. ABAQUS will then average all eight strains to produce a single time history. The time history for the bottom sensor of G3 and the table of it's data points are shown in the figure below. To access the data in a table format, right click on the saved XY Data file and select edit. The table can then be copied into another program to be processed.

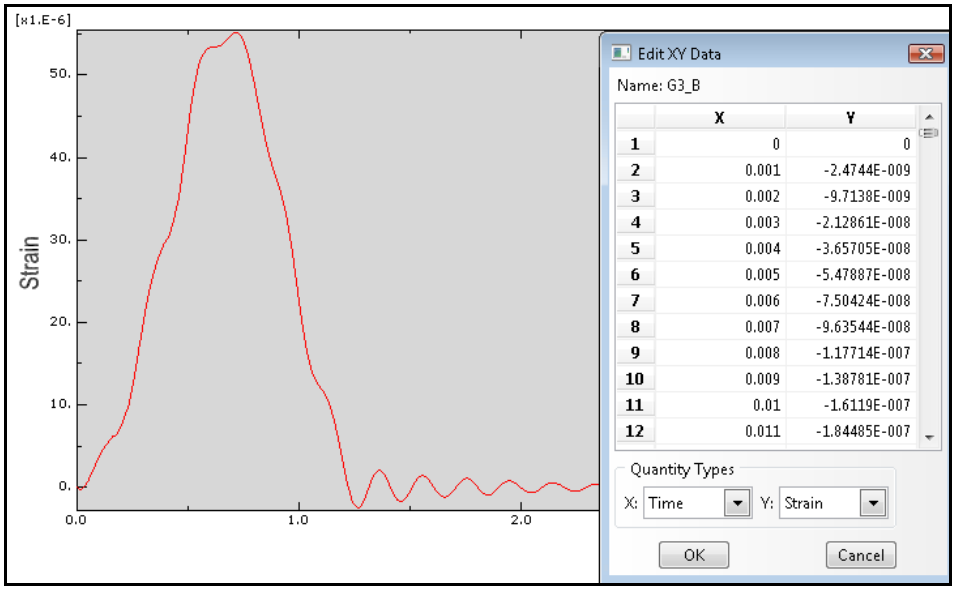

Figure 14. Plot and Table of G3 Bottom Node Strain

APPENDIX B: Dynamic Truck Loading

The bridge model is loaded using a five-axle 47ft truck with a 6ft wheelbase and a total weight of 69.76 kips (5). The truck was positioned so that it straddled Girder 3 to simulate a truck travelling in the right travel lane. The contact area for the tires was based AASHTO specifications and constitutes a moving area of 10 inches by 20 inches (12).

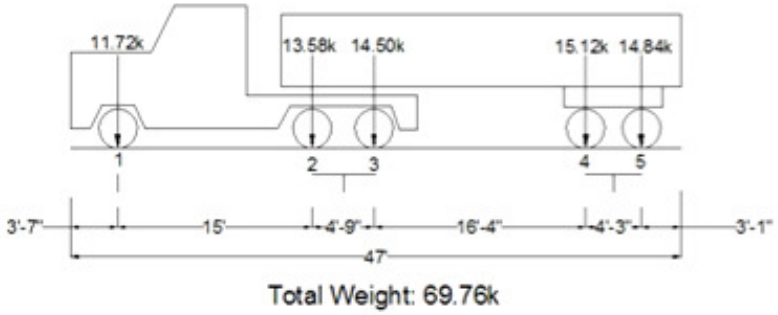

FIGURE 1. Configuration of Truck Used to Load Bridge.

In order to create the dynamic truck loading, the truck had to be incremented through both space and time in the finite element model. To model the physical incrimination of the truck, the length of the bridge deck was divided into 10" by 20" tributary tire areas. The five axles of the truck were then modeled physically as shown in Figure 2, below. In this figure, the blue squares represent Position A, the initial location the truck. To move the truck across the bridge, these loads were then incremented one space at a time across the length of the bridge as indicated by Positions B and C. In order to model the entire truck crossing, a total of 140 truck positions were modeled. Each tire position is assigned a distributed load corresponding to the axle weights given in Figure 1 shown above.

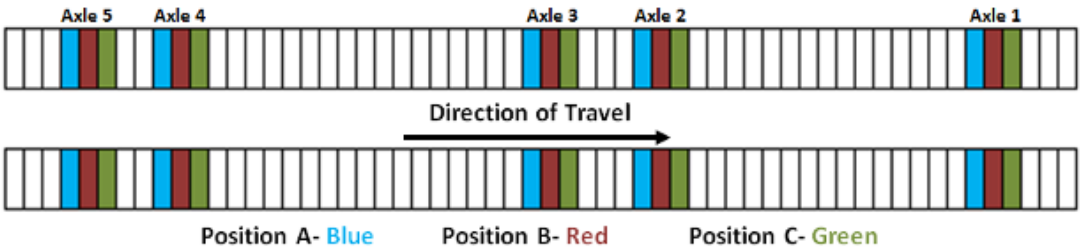

FIGURE 2. Physical Positioning of the Moving Truck

To increment the truck through time, each truck position was assigned a specific time history. Assigning a time history ensures that only one truck position is applied to the bridge at any given time. Since each tributary tire area is 10" long and the truck is assumed to be travelling at approximately 65mph, the truck takes 0.009 seconds to travel across the 10" length. This means that each truck location is held for a total of 0.009 seconds before the next load is applied. Figure 3 shows the time histories for the three truck positions shown in Figure 3, above. As is evident in this plot, each time history begins immediately after the previous time history. This ensures two things. One, that only one truck position is applied to the bridge at any given time; and two, that the next truck increment is applied immediately after the previous one creating a continuous loading.

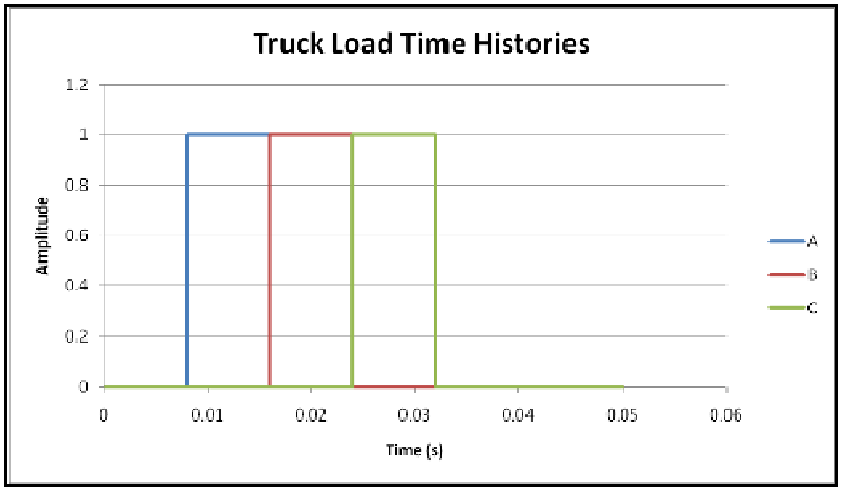

FIGURE 3. Time Histories of Three Consecutive Truck Positions

APPENDIX B: Complete Results of Finite Element Analysis

Complete Results for DM_{ε}

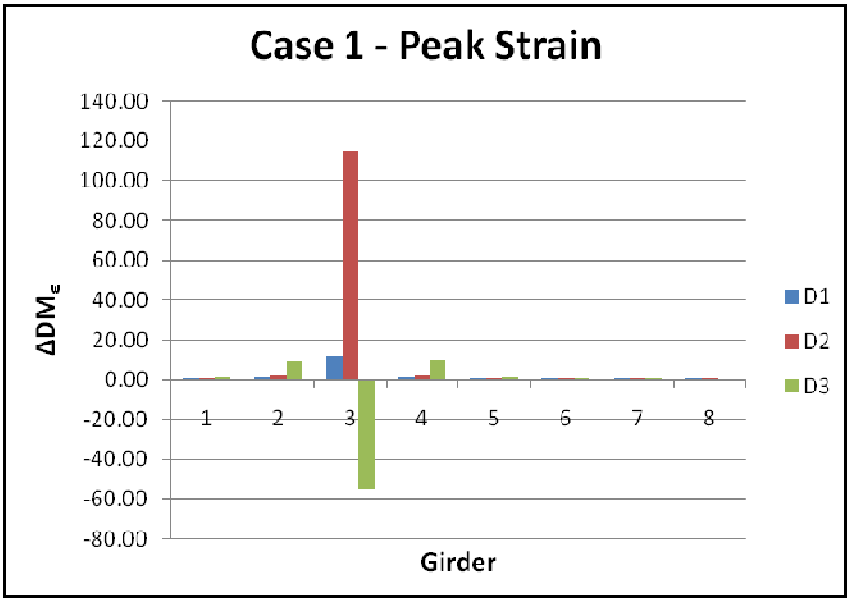

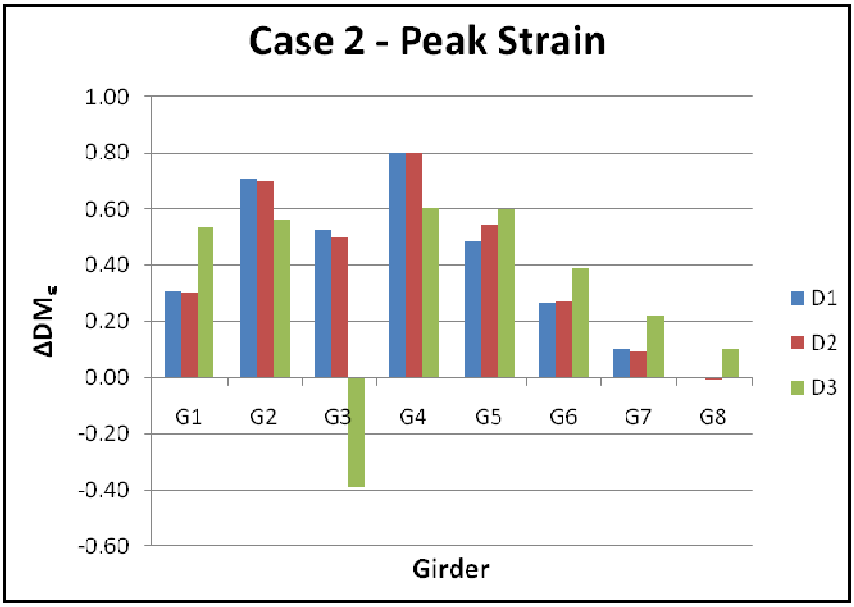

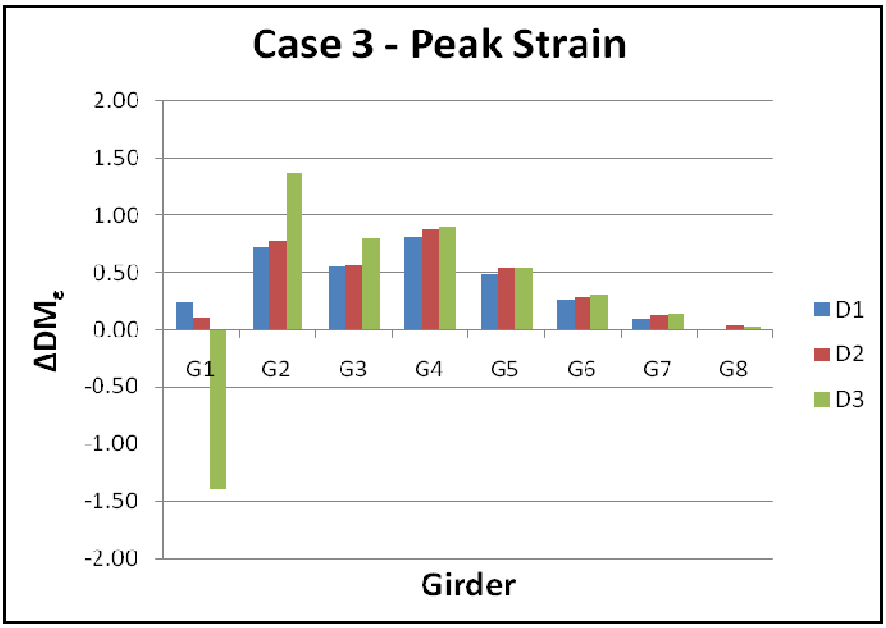
Case 3 - Peak Strain
2.00
1.50
1.00
0.50
0.00
-0.50
-1.00
-1.50
-2.00
ΔDM_ε
G1
G2
G3
G4
G5
G6
G7
G8
Girder
D1
D2
D3

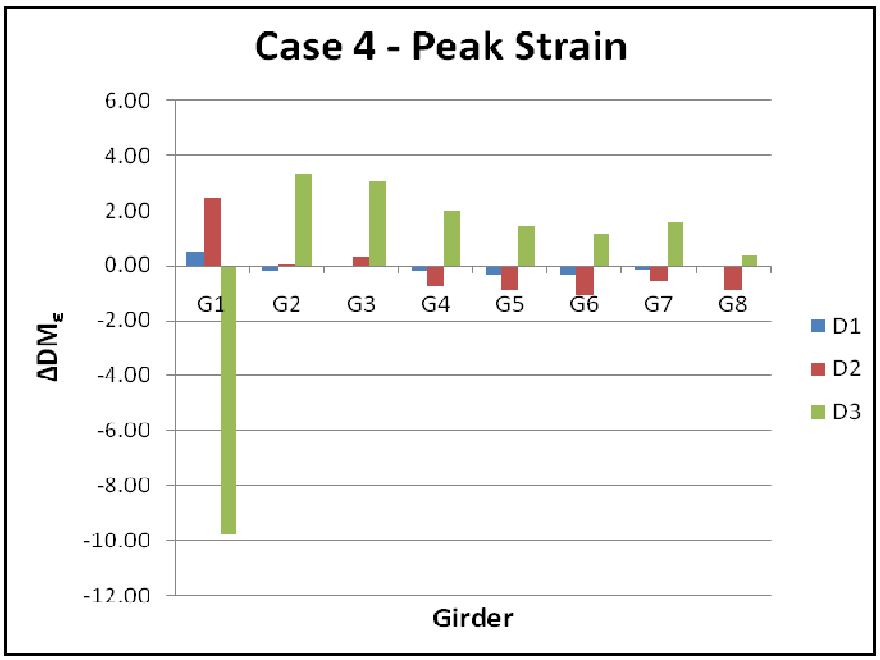
Case 4 - Peak Strain
6.00
4.00
2.00
0.00
-2.00
-4.00
-6.00
-8.00
-10.00
-12.00
ΔDM_ε
G1
G2
G3
G4
G5
G6
G7
G8
Girder
D1
D2
D3

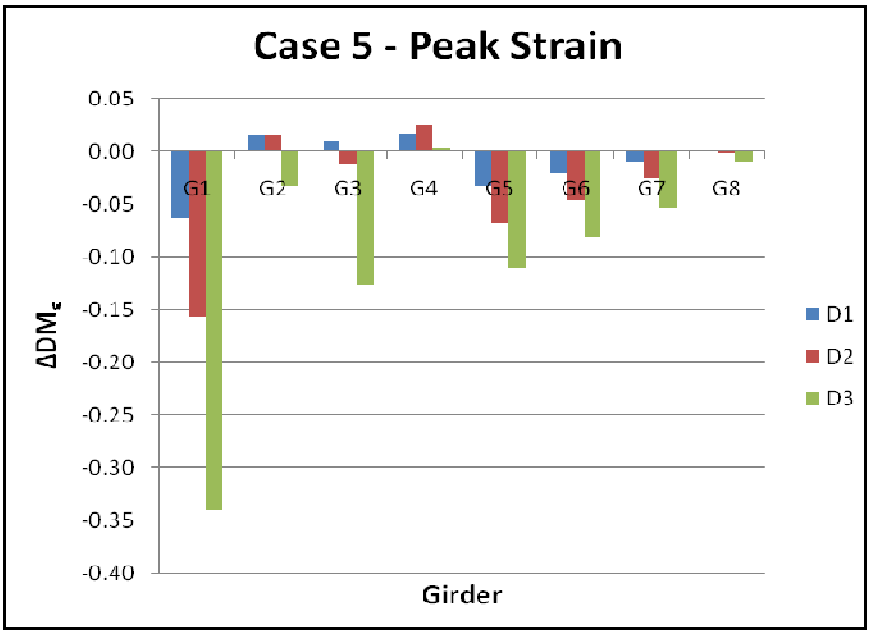

Complete Results for DM_{dist}

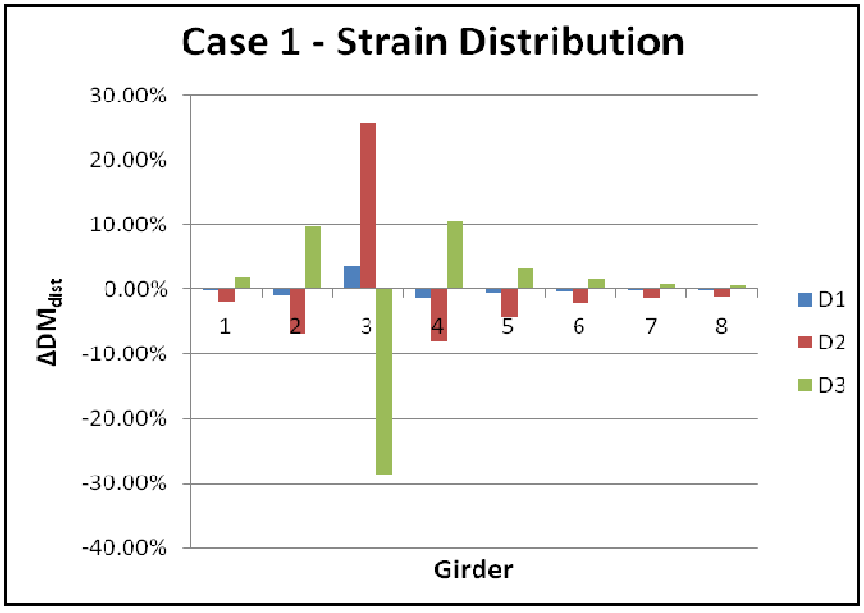

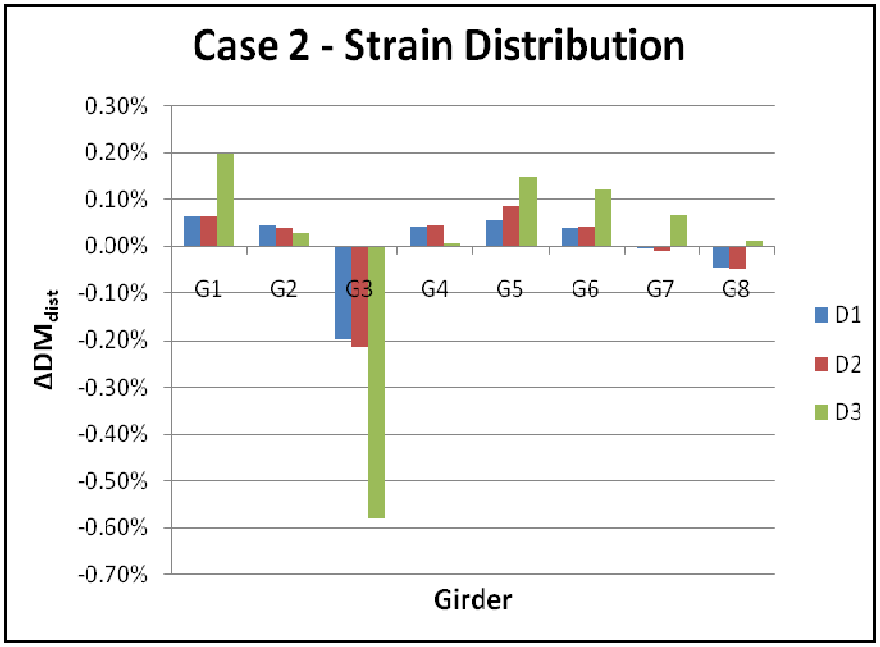
Case 2 - Strain Distribution
0.30%
0.20%
0.10%
0.00%
-0.10%
-0.20%
-0.30%
-0.40%
-0.50%
-0.60%
-0.70%
ΔDM_dist
G1
G2
G3
G4
G5
G6
G7
G8
Girder
D1
D2
D3

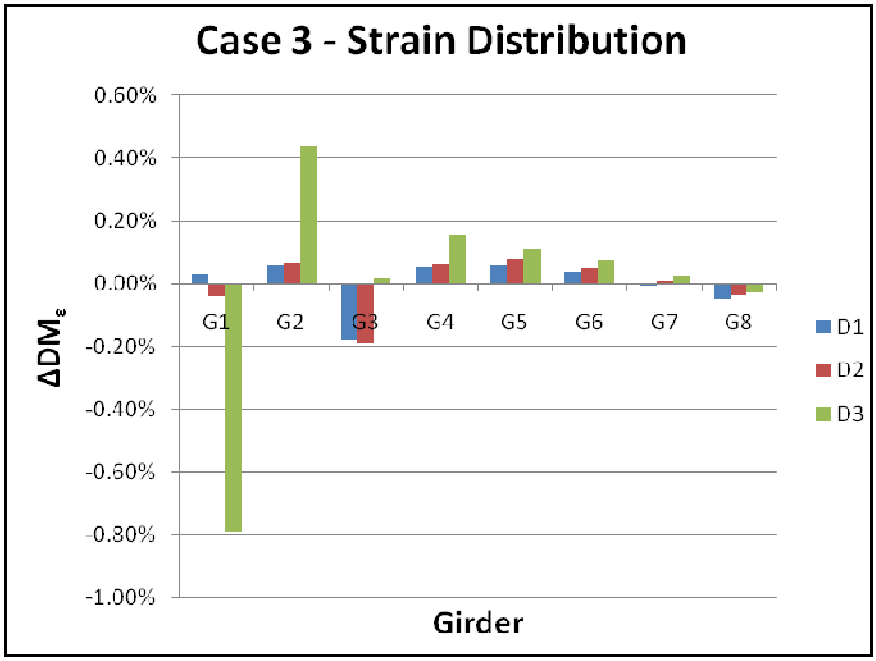
Case 3 - Strain Distribution
0.60%
0.40%
0.20%
0.00%
-0.20%
-0.40%
-0.60%
-0.80%
-1.00%
ΔDM_s
G1
G2
G3
G4
G5
G6
G7
G8
Girder
D1
D2
D3

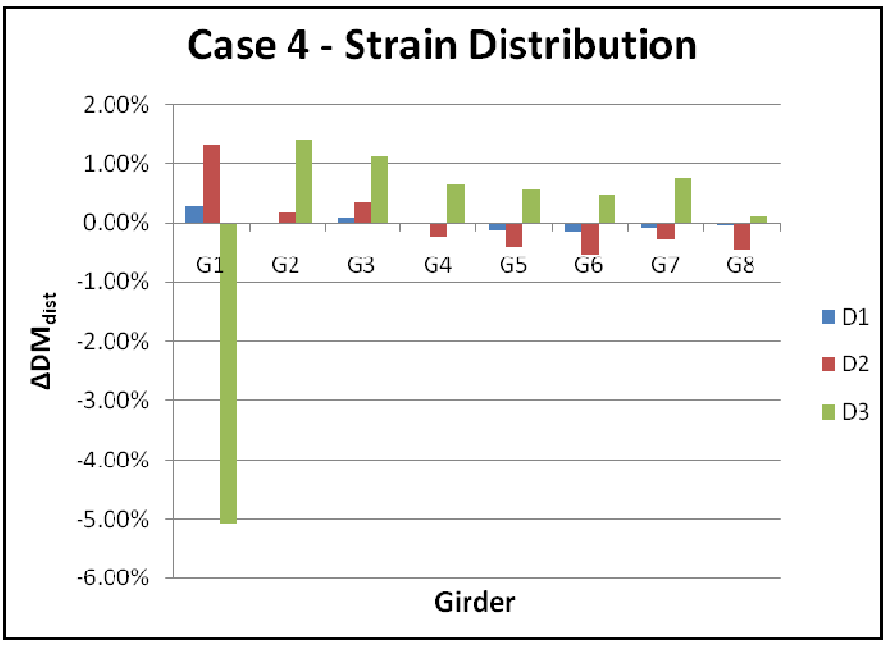
Case 4 - Strain Distribution
2.00%
1.00%
0.00%
-1.00%
-2.00%
-3.00%
-4.00%
-5.00%
-6.00%
G1
G2
G3
G4
G5
G6
G7
G8
ΔDMdist
Girder
D1
D2
D3

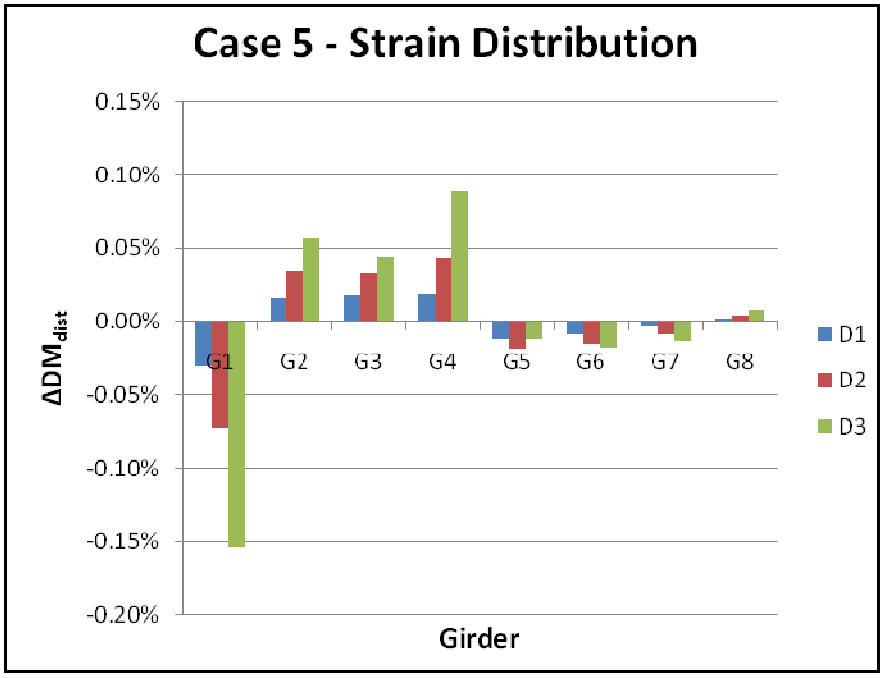
Case 5 - Strain Distribution
0.15%
0.10%
0.05%
0.00%
-0.05%
-0.10%
-0.15%
-0.20%
G1
G2
G3
G4
G5
G6
G7
G8
ΔDMdist
Girder
D1
D2
D3

Complete Results for DM_{NA}

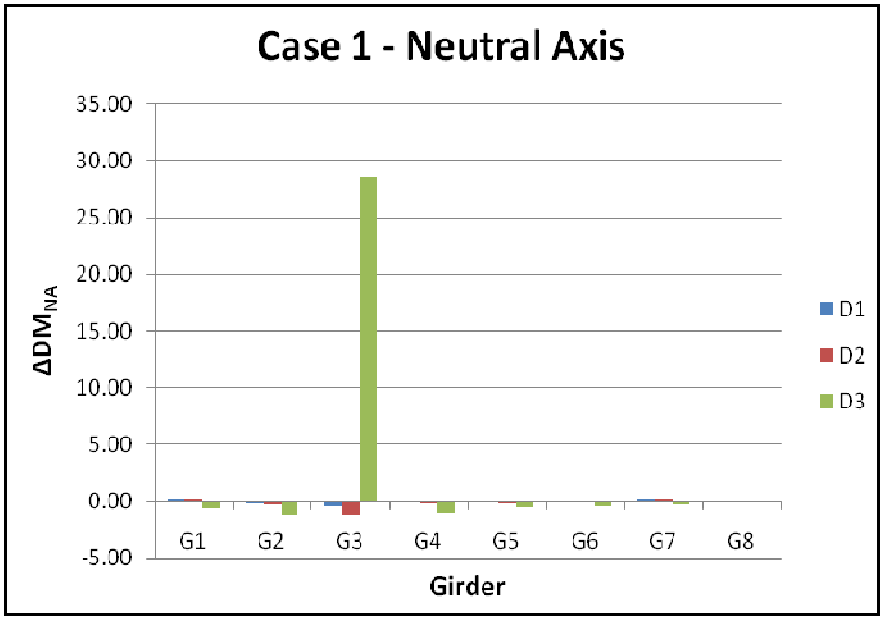

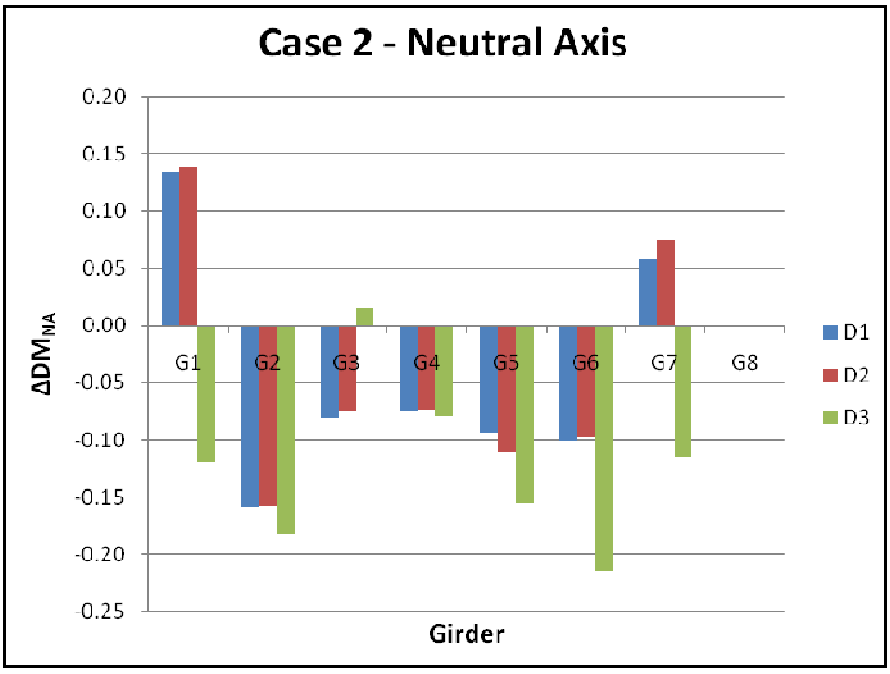

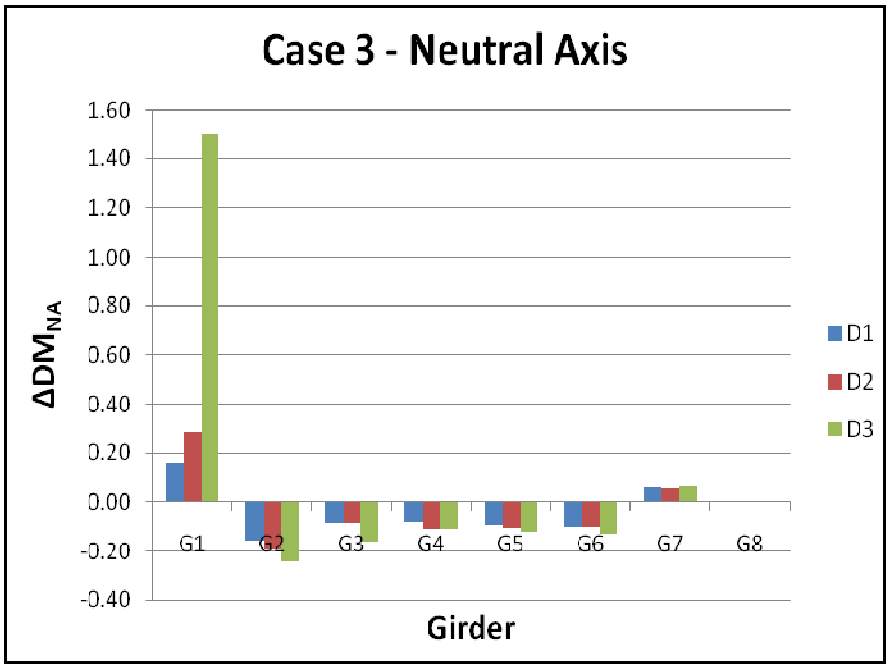
Case 3 - Neutral Axis
1.60
1.40
1.20
1.00
0.80
0.60
0.40
0.20
0.00
-0.20
-0.40
ΔDM_NA
G1
G2
G3
G4
G5
G6
G7
G8
Girder
D1
D2
D3

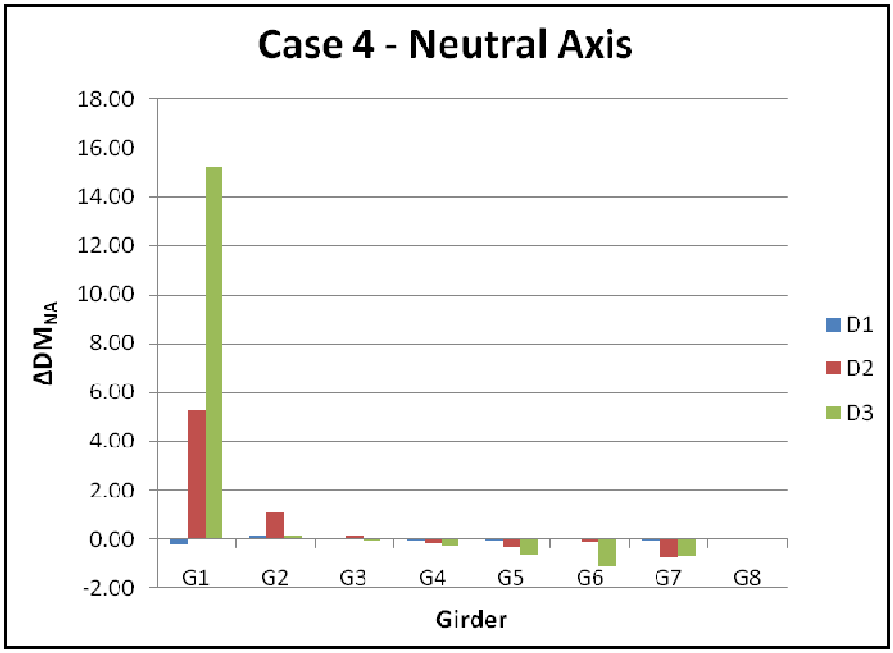
Case 4 - Neutral Axis
18.00
16.00
14.00
12.00
10.00
8.00
6.00
4.00
2.00
0.00
-2.00
ΔDM_NA
G1
G2
G3
G4
G5
G6
G7
G8
Girder
D1
D2
D3

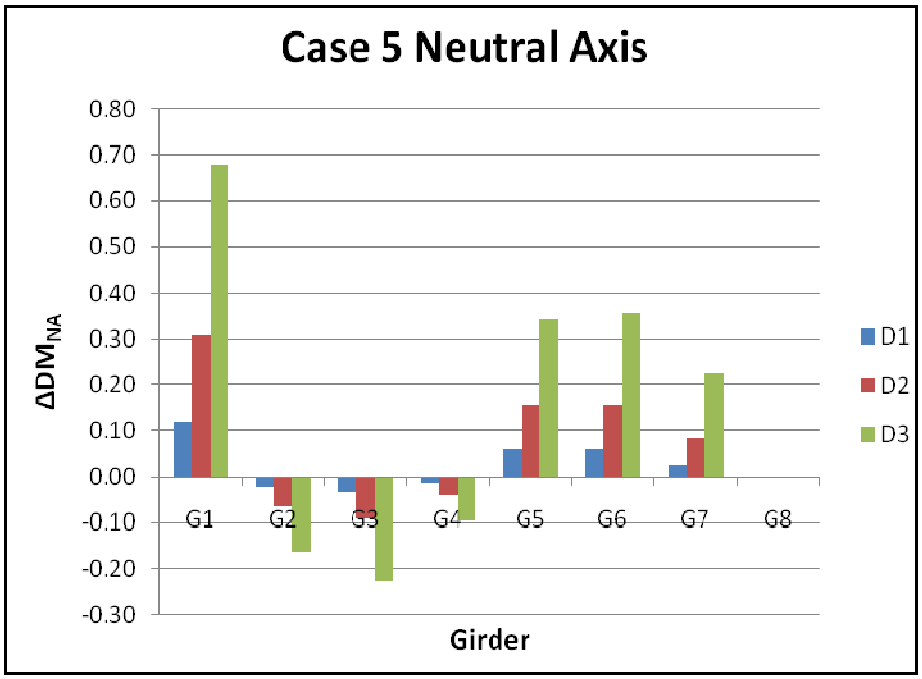
Case 5 Neutral Axis
0.80
0.70
0.60
0.50
0.40
0.30
0.20
0.10
0.00
-0.10
-0.20
-0.30
ΔDM_NA
G1
G2
G3
G4
G5
G6
G7
G8
Girder
D1
D2
D3

APPENDIX C- Uncertainty of Damage Measures

Uncertainty of Peak Strain Damage Measure

P-Values for the Peak Strain Damage Measures

Girder	P-Value (%)
G1	1.9516x10-9
G2	3.5538x10-4
G3	3.1894x10-8
G4	5.7948x10-5
G5	2.1861x10-5
G6	6.9208x10-6
G7	1.2487x10-5
G8	0.0038

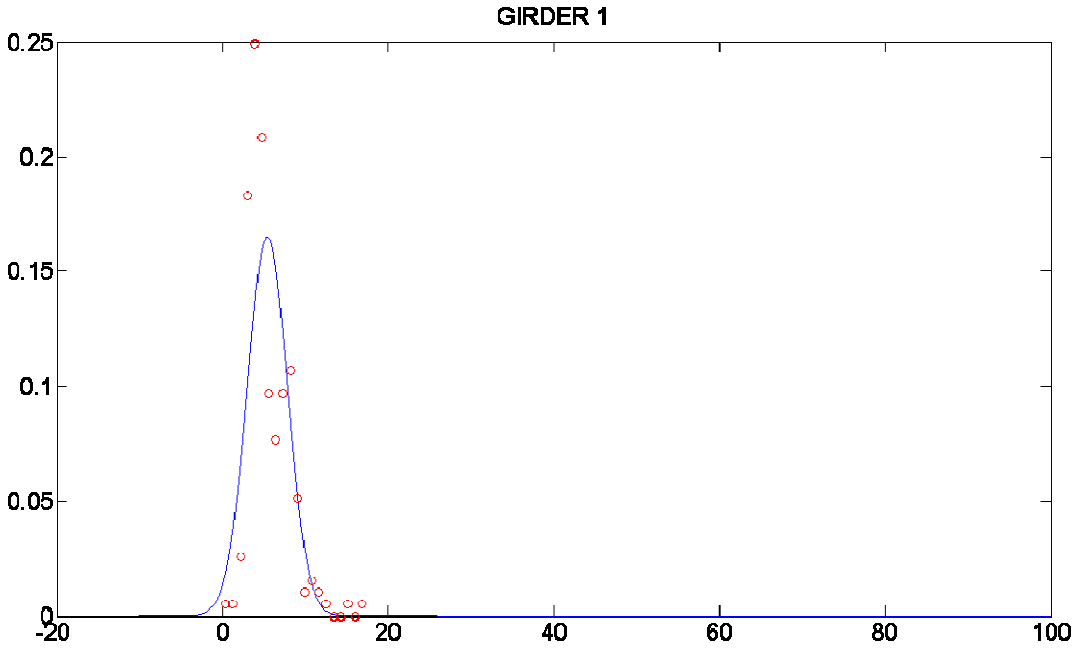

Probability Density Function vs. Histogram of Recorded Data- Peak Strain G1

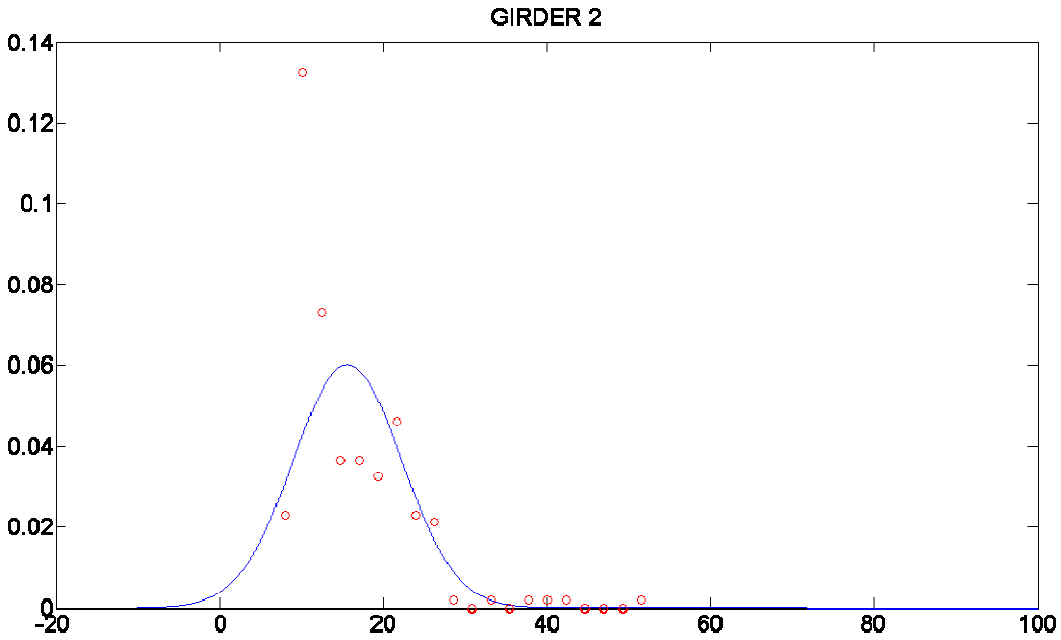

Probability Density Function vs. Histogram of Recorded Data- Peak Strain G2

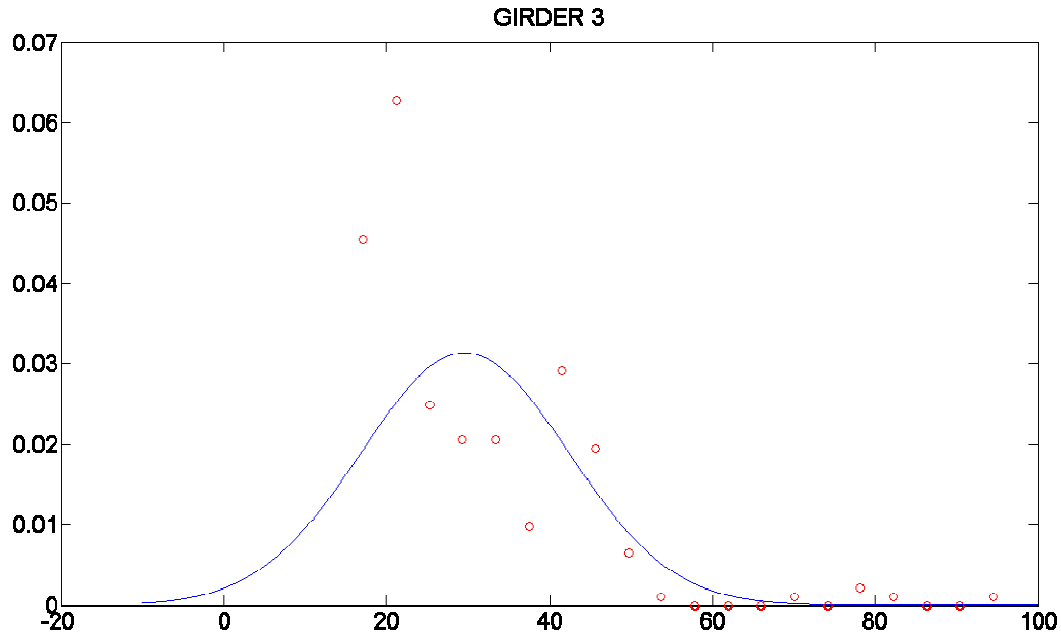

Probability Density Function vs. Histogram of Recorded Data- Peak Strain G3

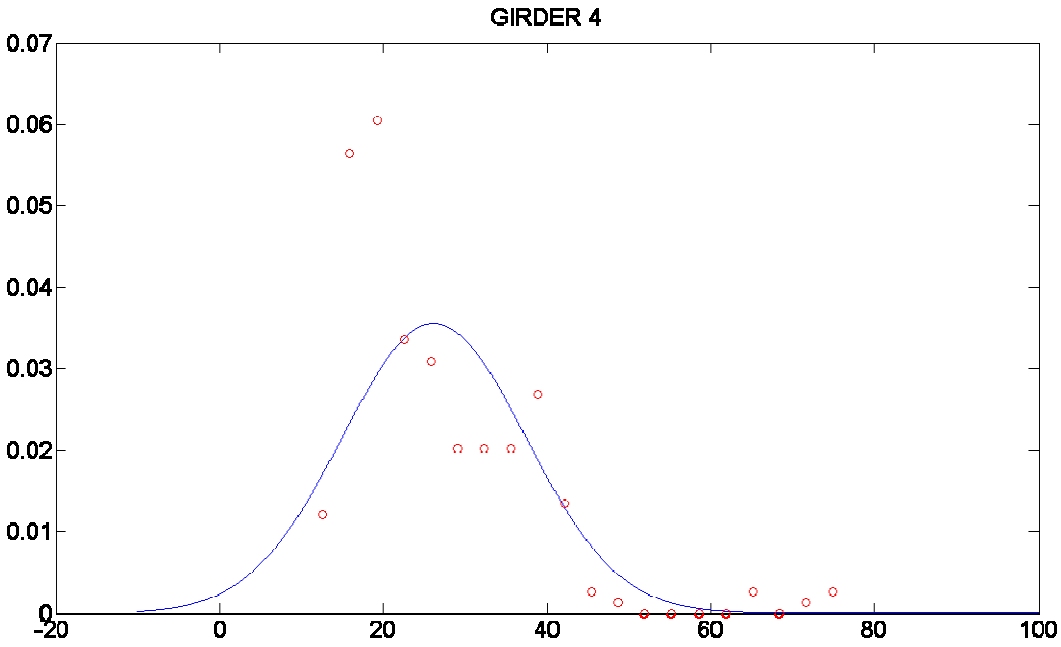

Probability Density Function vs. Histogram of Recorded Data- Peak Strain G4

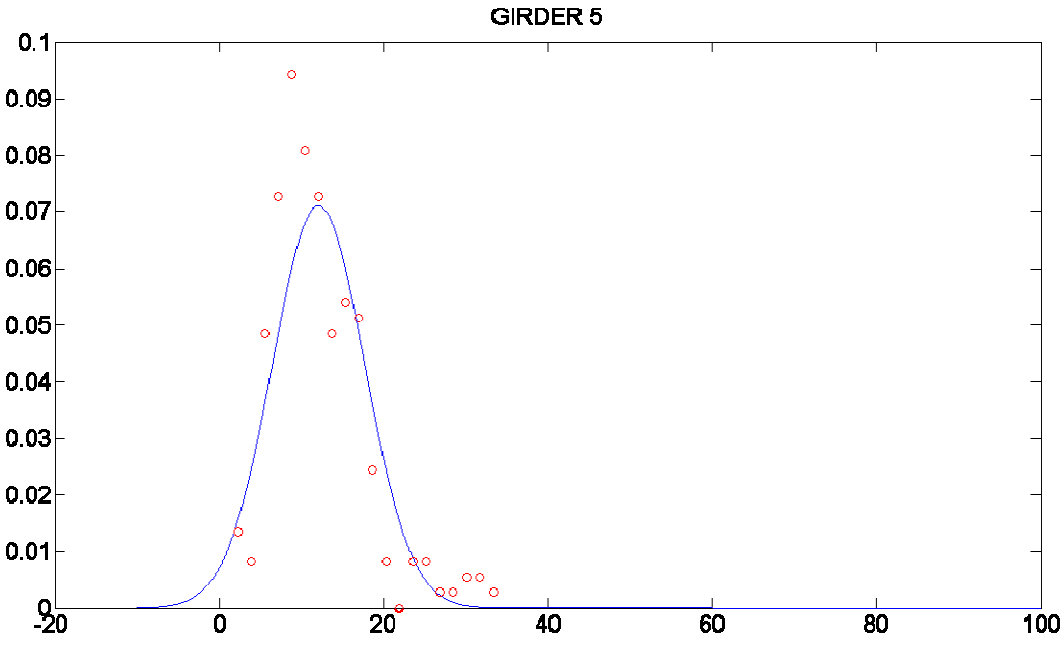

Probability Density Function vs. Histogram of Recorded Data- Peak Strain G5

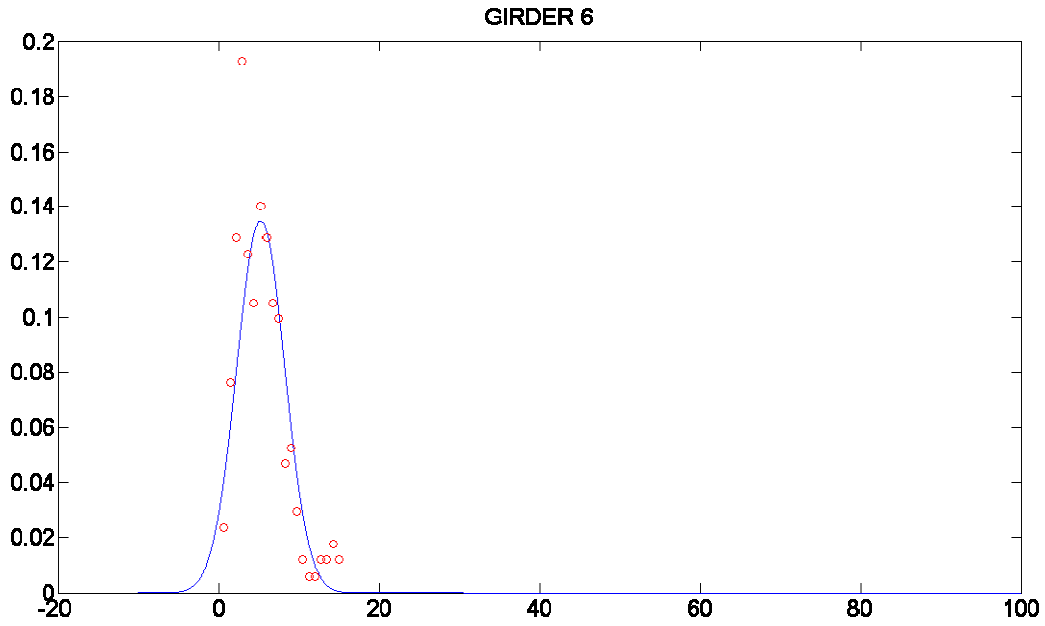

Probability Density Function vs. Histogram of Recorded Data- Peak Strain G6

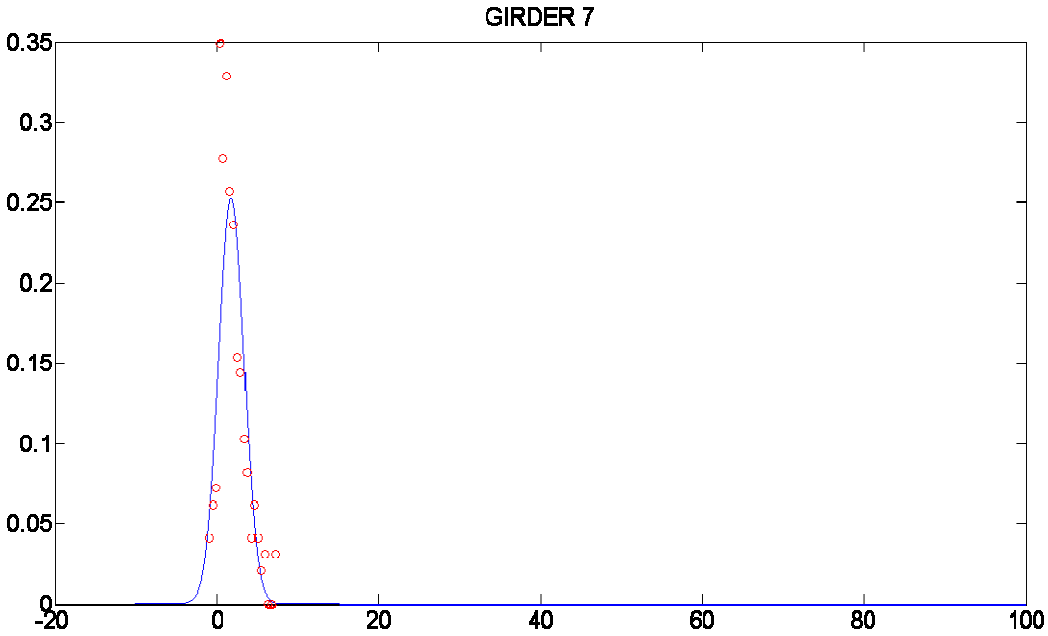

Probability Density Function vs. Histogram of Recorded Data- Peak Strain G7

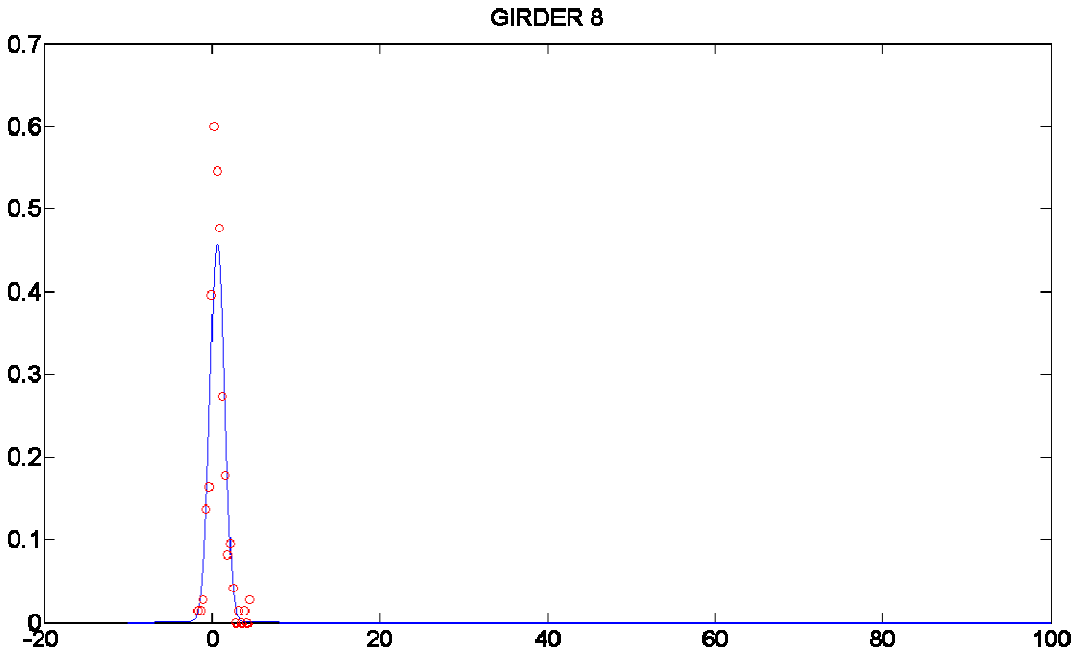

Probability Density Function vs. Histogram of Recorded Data- Peak Strain G8

Uncertainty of Strain Distribution Damage Measure

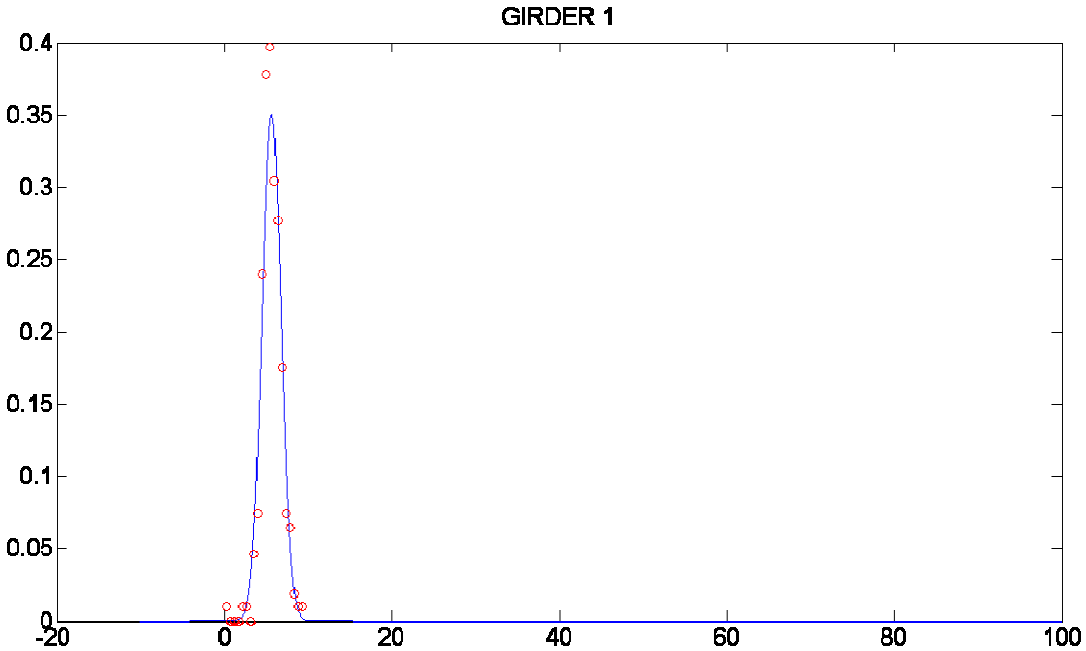

Probability Density Function vs. Histogram of Recorded Data- Strain Distribution G1

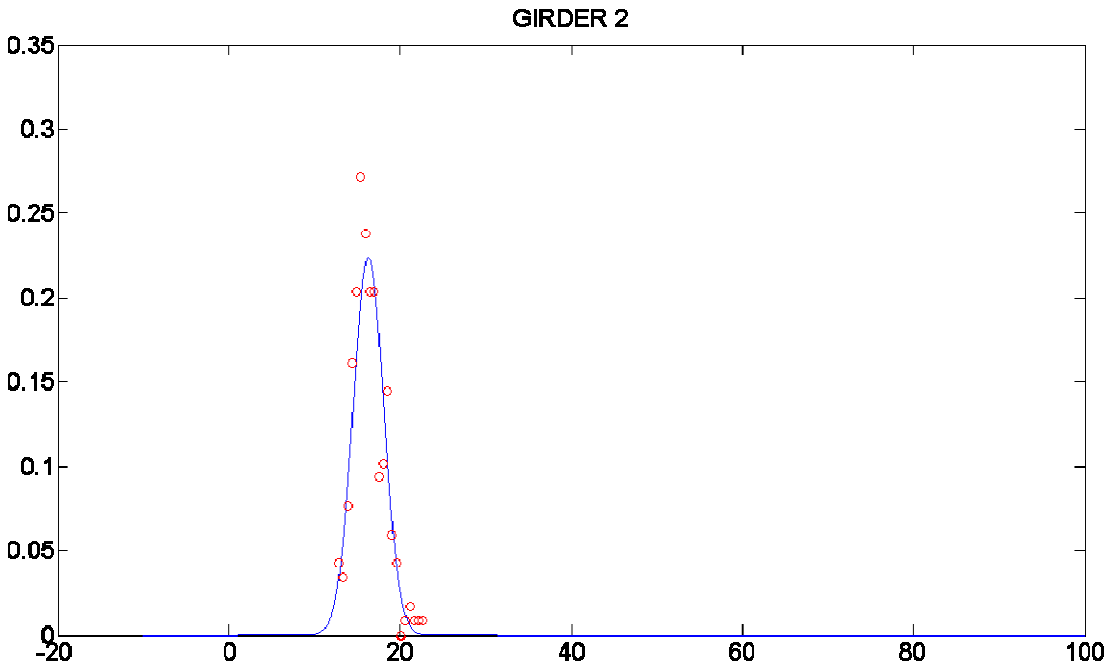

Probability Density Function vs. Histogram of Recorded Data- Strain Distribution G2

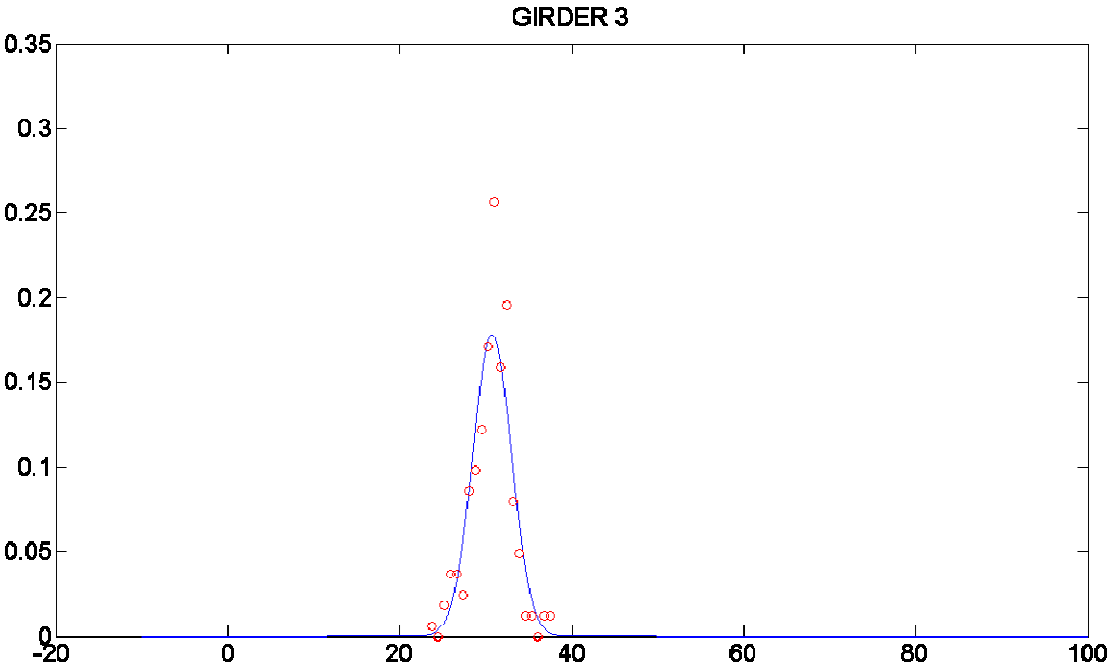

Probability Density Function vs. Histogram of Recorded Data- Strain Distribution G3

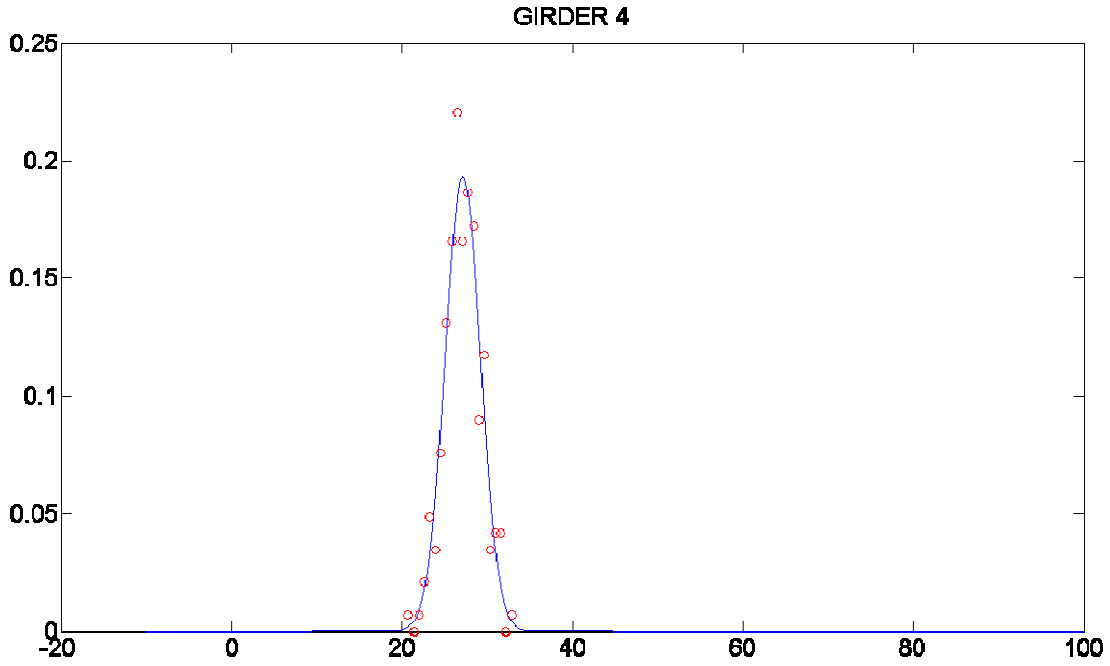

Probability Density Function vs. Histogram of Recorded Data- Strain Distribution G4

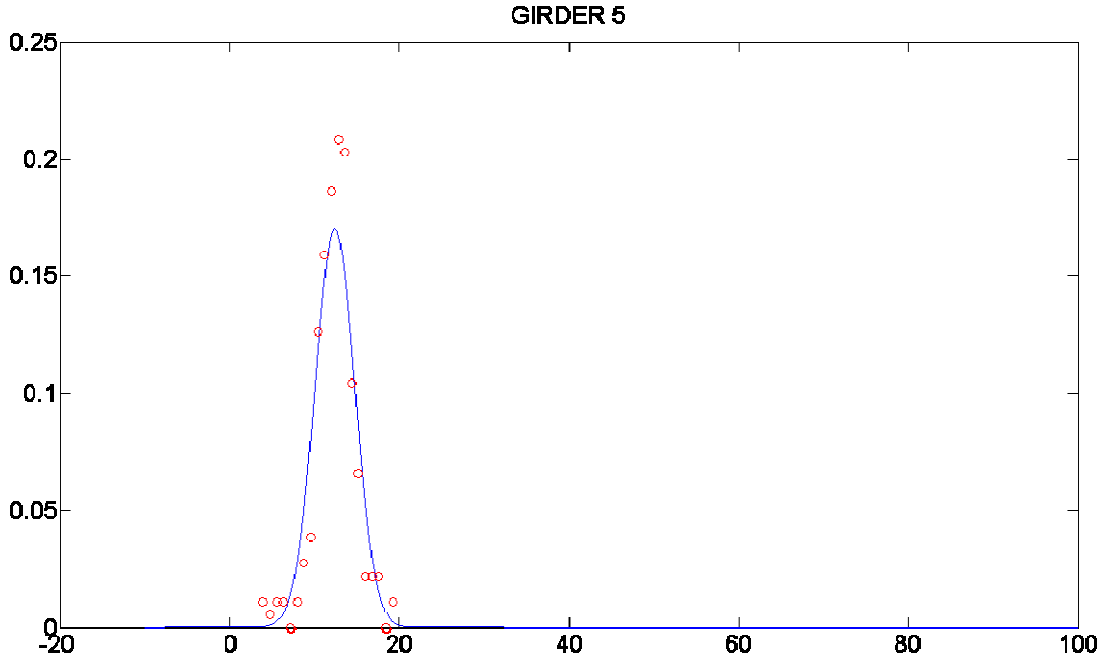

Probability Density Function vs. Histogram of Recorded Data- Strain Distribution G5

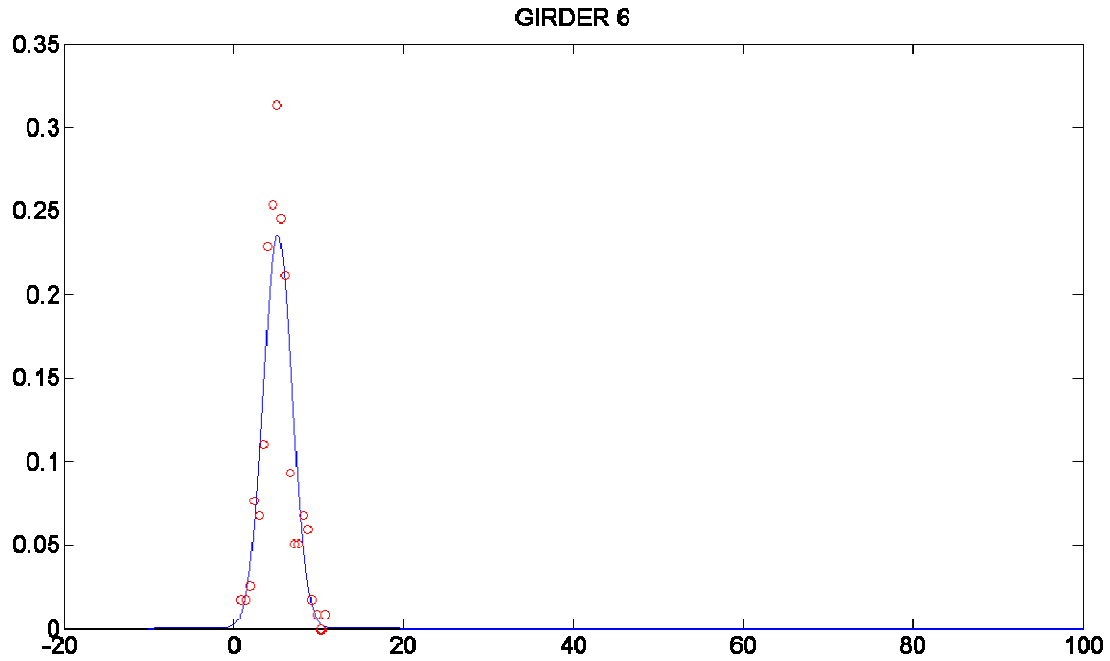

Probability Density Function vs. Histogram of Recorded Data- Strain Distribution G6

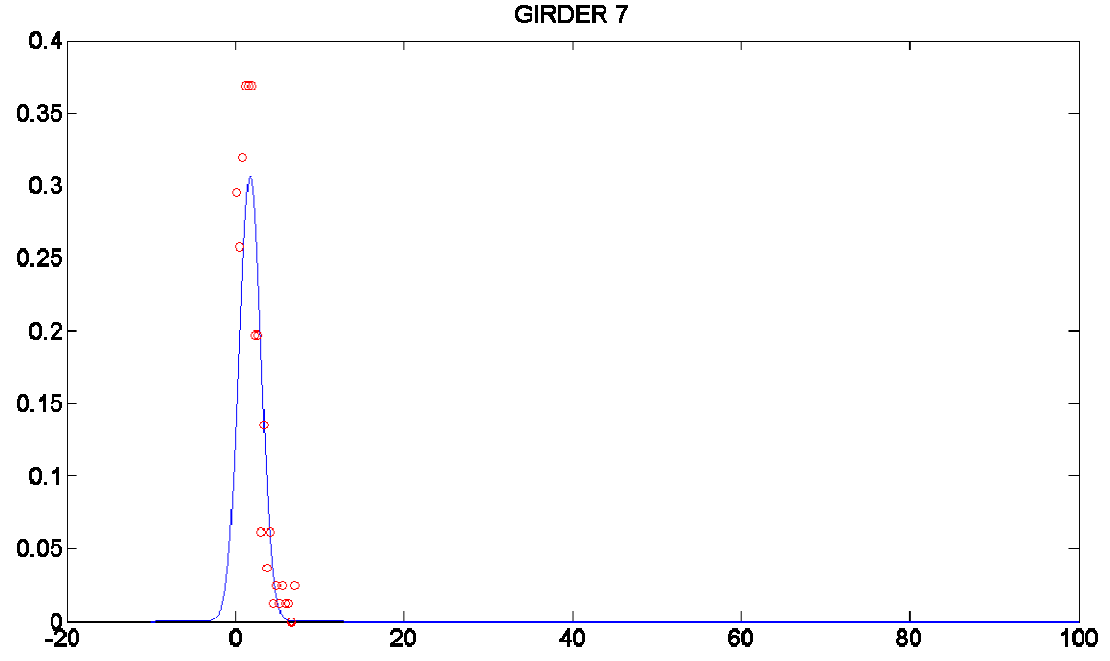

Probability Density Function vs. Histogram of Recorded Data- Strain Distribution G7

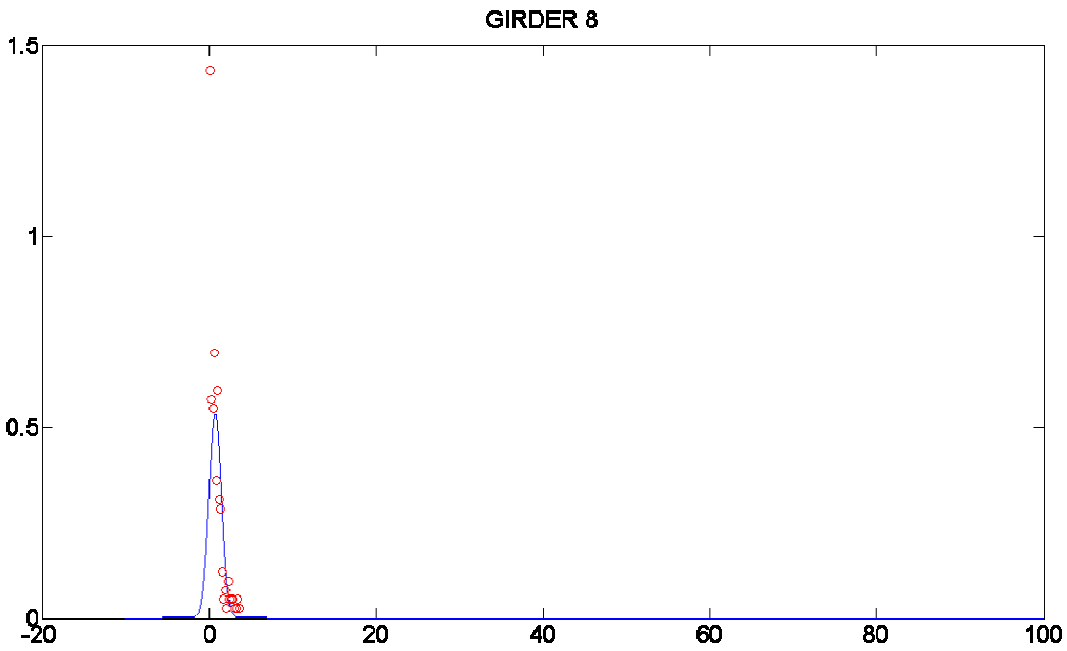

Probability Density Function vs. Histogram of Recorded Data- Strain Distribution G8

Uncertainty of Neutral Axis Damage Measure

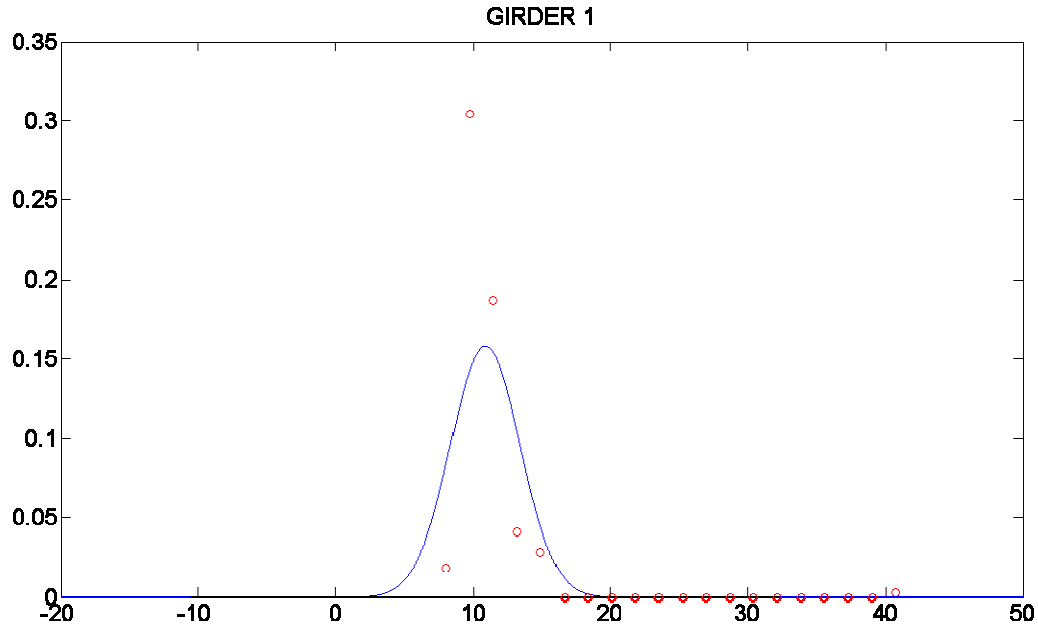

Probability Density Function vs. Histogram of Recorded Data- Neutral Axis G1

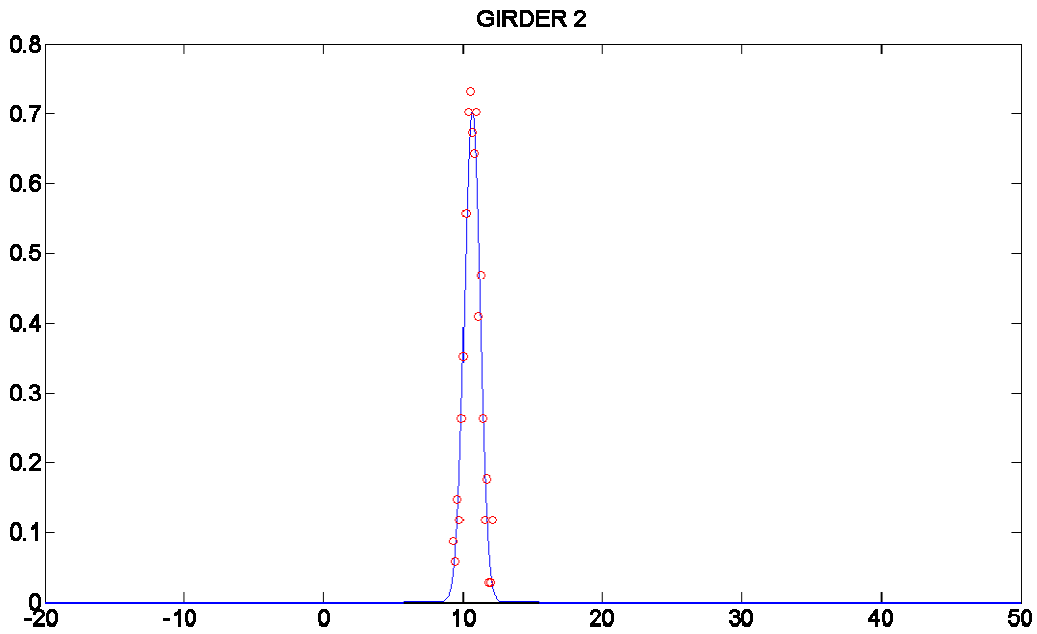

Probability Density Function vs. Histogram of Recorded Data- Neutral Axis G2

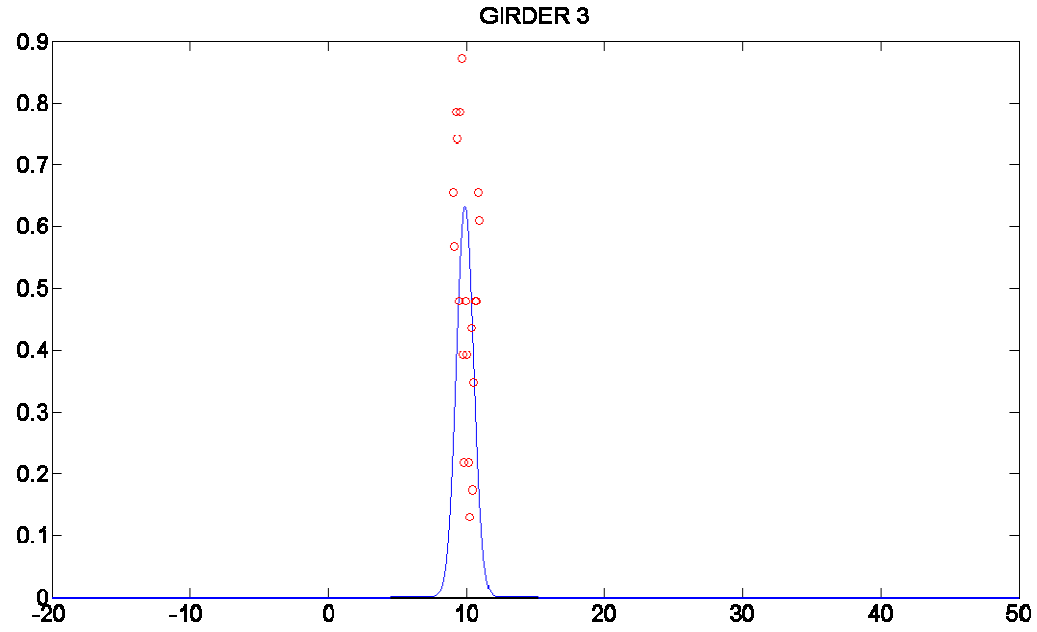

Probability Density Function vs. Histogram of Recorded Data- Neutral Axis G3

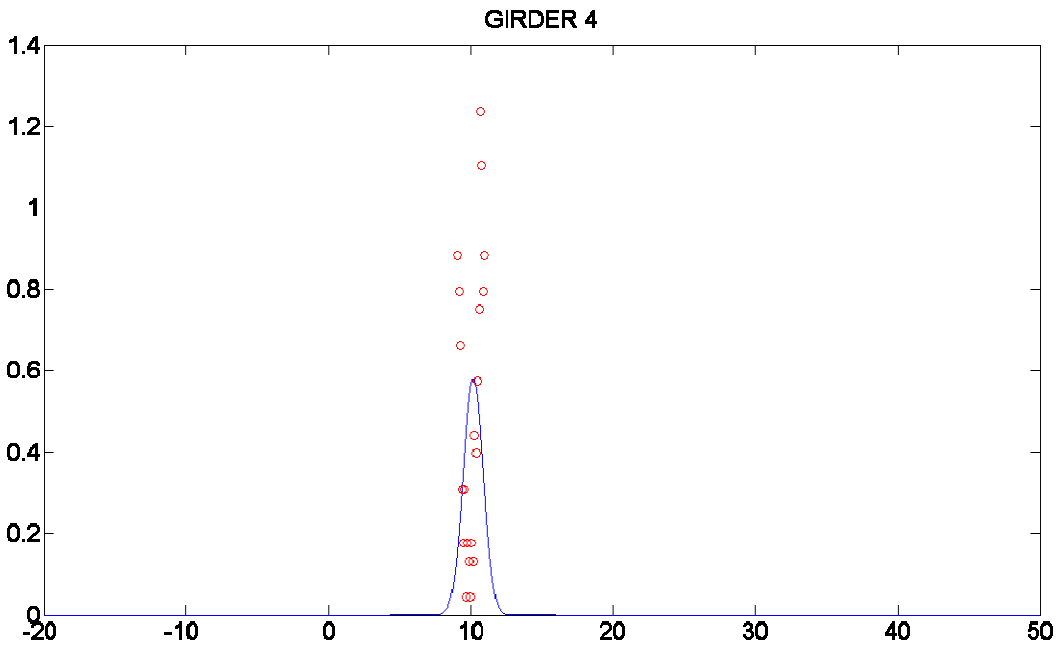

Probability Density Function vs. Histogram of Recorded Data- Neutral Axis G4

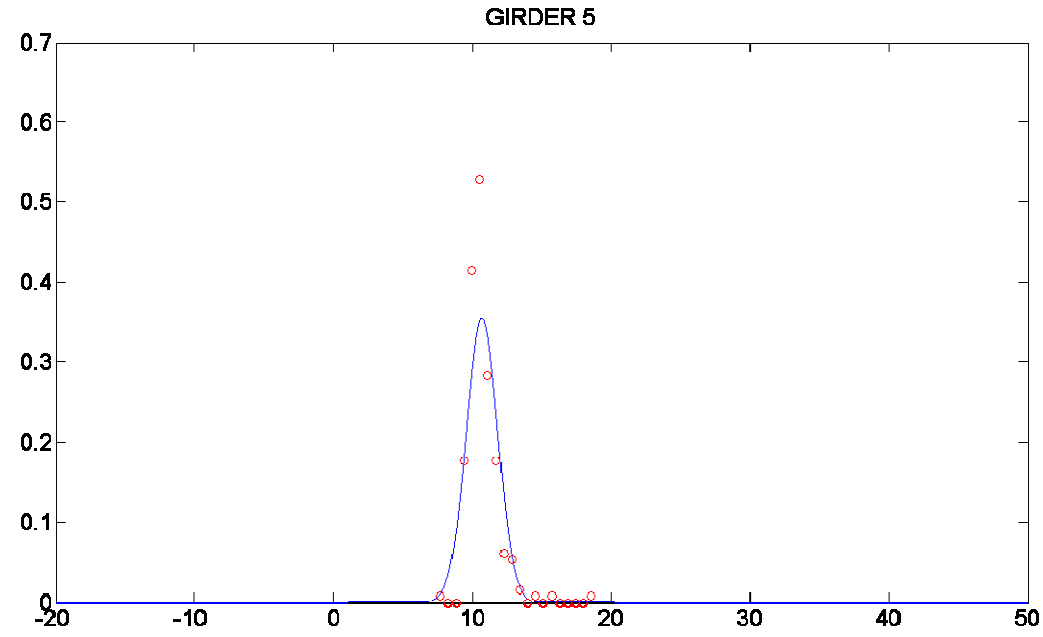

Probability Density Function vs. Histogram of Recorded Data- Neutral Axis G5

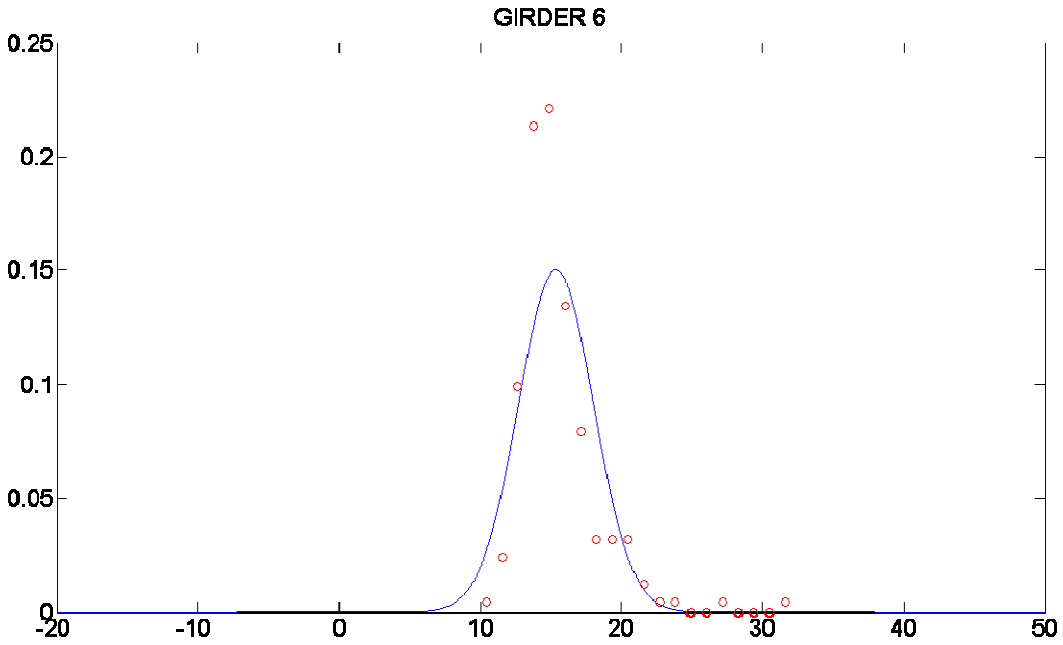

Probability Density Function vs. Histogram of Recorded Data- Neutral Axis G6

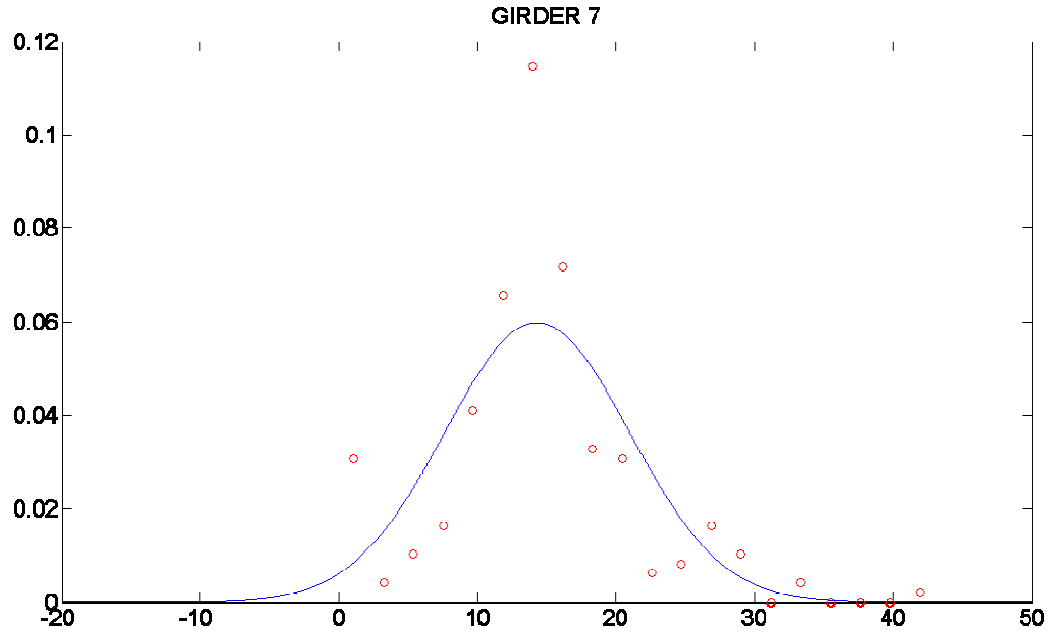

Probability Density Function vs. Histogram of Recorded Data- Neutral Axis G7

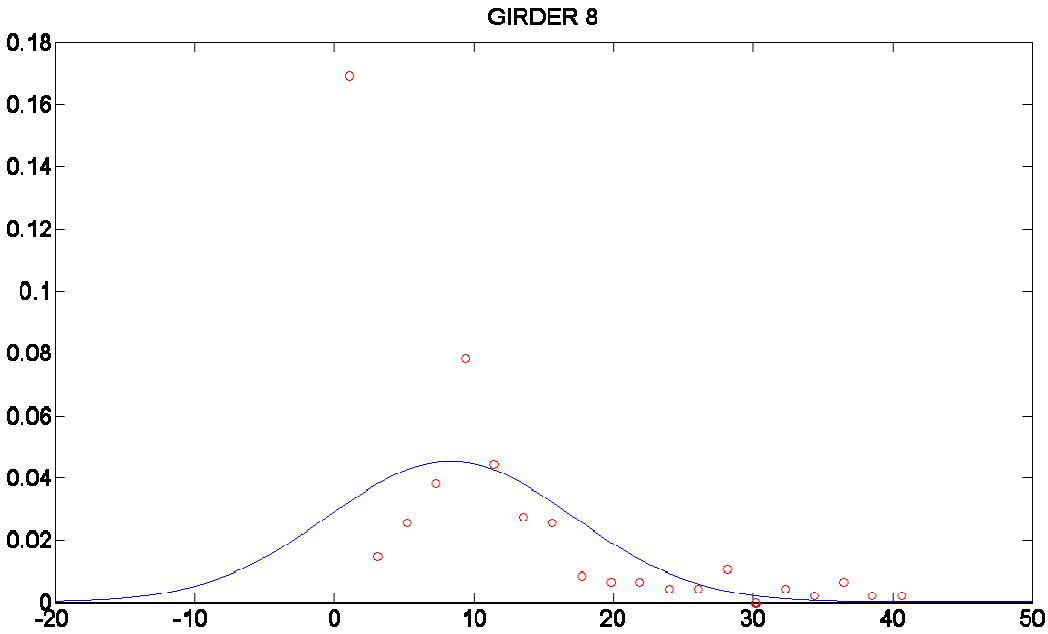

Probability Density Function vs. Histogram of Recorded Data- Neutral Axis G8